University of Genoa

Department of Experimental Medicine

Master Degree in

MEDICAL-PHARMACEUTICAL BIOTECHNOLOGY

Characterization of fetal and perinatal human amniotic fluid-derived progenitor cells: analysis of their secretome fractions and paracrine potential for myocardial renewal

Supervisors:

Assoc. Prof. Sveva Bollini

Ass. Prof. Silvia Ravera

Dept. of Experimental Medicine

Candidate:

Sara Turturo

(Matr.s4258070)

Academic Year 2020/2021

INDEX

SUMMARY

In recent years stem cell paracrine effects have emerged as an appealing strategy in experimental research for regenerative medicine. Independent preclinical studies have revealed a promising therapeutic role in the stem and progenitor cell secretome, as the composite set of paracrine trophic factors and extracellular vescicles (EVs) released by them. These secreted soluble factors have been shown to influence the microenvironment at the site of injury by triggering endogenous mechanism of recovery, leading to functional improvement of the damaged organ or tissue[1,2]. In order to clinically translate such paracrine approach, it is fundamental to determine the most suitable stem/progenitor cell source, based on their isolation feasibility, self-renewal capacity, and paracrine regenerative potential.

Human amniotic fluid-derived stem cells (hAFS) have been broadly described as endowed with high self-renewal potential; they can be obtained from leftover samples of II trimester amniotic fluid from routine amniocentesis (namely fetal hAFS) or from clinical waste III trimester samples during scheduled C (Caesarean)-section delivery (perinatal hAFS). Furthermore, the fetal hAFS paracrine activity has been shown to exert a cardioprotective effect on rodent ischemic myocardium and on cardiac cells exposed to cardiotoxicity[3,4], with their secreted extracellular vesicles (hAFS-EVs) mediating pro-survival, proliferative, and anti-inflammatory influence on target cells[3]. Noteworthy, both the fetal hAFS-conditioned medium (hAFS-CM) and the corresponding hAFS-EVs have been demonstrated to improve cardiac function and support resident surviving cardiomyocyte cell cycle re-entry in a preclinical mouse model of myocardial infarction (MI)[5].

In light of such evidence, during my thesis internship I have been involved in a study on the comprehensive characterisation of the hAFS secretome fractions and their validation to stimulate myocardial renewal by means of cardiomyocyte proliferation. In this scenario, a critical aspect is represented by the evaluation of the putative influence of gestational stage in modulating hAFS secretory activity. Although little is known about III trimester perinatal hAFS, they could represent an easy-to access alternative to II trimester fetal ones. Thus, my activity has been focused on the analysis of perinatal hAFS versus fetal hAFS, including their secretome fractions (i.e. the cell-conditioned medium, hAFS-CM and the released extracellular vesicles, hAFS-EVs) following hypoxic cell preconditioning as stimulatory approach to enrich their paracrine content. *In vitro* investigation of fetal- vs perinatal hAFS secretome fraction potential in stimulating myocardial renewal was performed on cardiomyocyte primary culture obtained from a transgenic mouse model endowed with fluorescently tagged cell cycle probe system.

From the results obtained so far, while gestational stage was shown not to influence either hAFS phenotype or secretory activity, the protein and chemokine/cytokine content of fetal and perinatal hAFS secretome formulations presented distinct profiles. Indeed, the more immature fetal hAFS secretome obtained following cell hypoxic preconditioning, presented a more pronounced pro-angiogenic, anti-ageing and pro-resolving paracrine potential. *In vitro* analysis on primary murine cardiomyocytes revealed a significant 2-fold increase in the cells progressing from S-phase up to M-phase of the cell cycle when stimulated by fetal hAFS-EVs only. Moreover, cytokinetic events within treated cardiomyoctes were also enhanced by 4.5-fold under the paracrine influence of fetal hAFS-EVs. Proteomic characterization of fetal hAFS-EVs revealed an exclusive enrichment in agrin, an extracellular matrix protein well-known for exerting cardiomyogenic effects[6], thus suggesting a possible molecular candidate underlying such stimulatory influence.

Further analyses are needed to better pinpoint the mechanism of action of fetal hAFS-EVs in stimulating cardiomyocyte renewal and to confirm such effect *in vivo* in a preclinical mouse model of cardiac injury with reliable assessment of cell cycle progression.

1 INTRODUCTION

1.1 Stem cells in regenerative medicine: from plasticity to paracrine effects

In the last years regenerative medicine has fast developed as experimental field to provide restoration of tissues and organs damaged by age, disease, or trauma, with hope to decrease reliance on transplantation therapy, which suffers from limited donor supply and may present severe immune complications[7]. Among the several strategies adopted by regenerative medicine, stem-cell therapy has been long investigated with the goal of replacing affected/damaged/dead cells within a tissue or an organ with newly obtained functional ones via stem cell trans-differentiation. Despite the initial excitement and high expectations, an increasing number of preclinical studies have demonstrated that administration of stem cells or progenitor cells by transplantation into an injured organ or via systemic infusion resulted in low incidence and poor efficiency of their survival and therapeutically relevant level of engraftment, with poor acquisition of the desired functional phenotype by differentiation *in vivo*, especially when considering the cardiovascular background[1,8–10]. However, a growing body of evidence has shown that the tissues treated with the transplanted or infused stem cells showed promising sign of functional improvement, regardless the formation of new viable cells to replace the damaged ones. Given that, it is now clear that the basis of this functional recovery is not by means of progenitor cell plasticity and their differentiation potential[11], rather via the secretion of the composite set of cytokines, chemokines and growth/trophic factors, as well as membrane-bound extracellular vesicles - all together defined as *secretome* – that stem and progenitor cells can release. Indeed, the stem cell secretome has been demonstrated to be able to orchestrate many biological activities on the damaged tissue and it is considered more critical than the differentiation potential of the cells[12]. In particular, the stem/progenitor cell secretome role on tissue repair occurs through the modulation of the local environment, promoting pro-survival and anti-apoptotic effects, while influencing the immune/inflammatory response, sustaining local angiogenesis and establishing co-operative effects with the resident cells, overall resulting in a significant cytoprotective and pro-survival beneficial influence. Furthermore, the secretome may act either directly or indirectly on injured cells triggering neighboring cells to also secrete bioactive molecules. Direct evidence that stem cell-derived secretome plays a key role in mediating the regenerative effects observed *in vivo* has been demonstrated by a consistent body of studies on cardiac, renal, liver and lung injury, as well as in neurodegenerative disease models[12–16].

Cardiovascular disease has become of particular interest in the scenario of paracrine effects from progenitor stem cells. As a matter of fact, cardiovascular disease still represents the leading cause of

mortality and morbidity worldwide[17]. Specifically, ischemic-related myocardial infarction represents one of the most common causes of cardiac dysfunction and the pathological basis for the development of heart failure over time. When facing prolonged ischemia, the mammalian adult myocardial tissue can only activate a defective repair mechanism aiming at replacing the dead cardiomyocytes with a fibrotic collagen scar, leading over time to the surviving cardiomyocyte (CM) hypertrophy and to the pathological remodelling of the cardiac chambers, overall resulting in heart failure. Despite the most recent progresses of interventional cardiology combined to prompt pharmacological treatment, cardiac regeneration by functional myocardial renewal is yet not possible and heart transplantation still represents the ultimate therapeutic option[18,19].

Against this scenario, in the last 15 years several stem- and mesenchymal stromal cell populations have shown to exert remarkable paracrine cardioprotective, provasculogenic, anti-inflammatory, antifibrotic effects with relevant beneficial effect on the infarcted heart [8,12,20–24] (Figure 1).

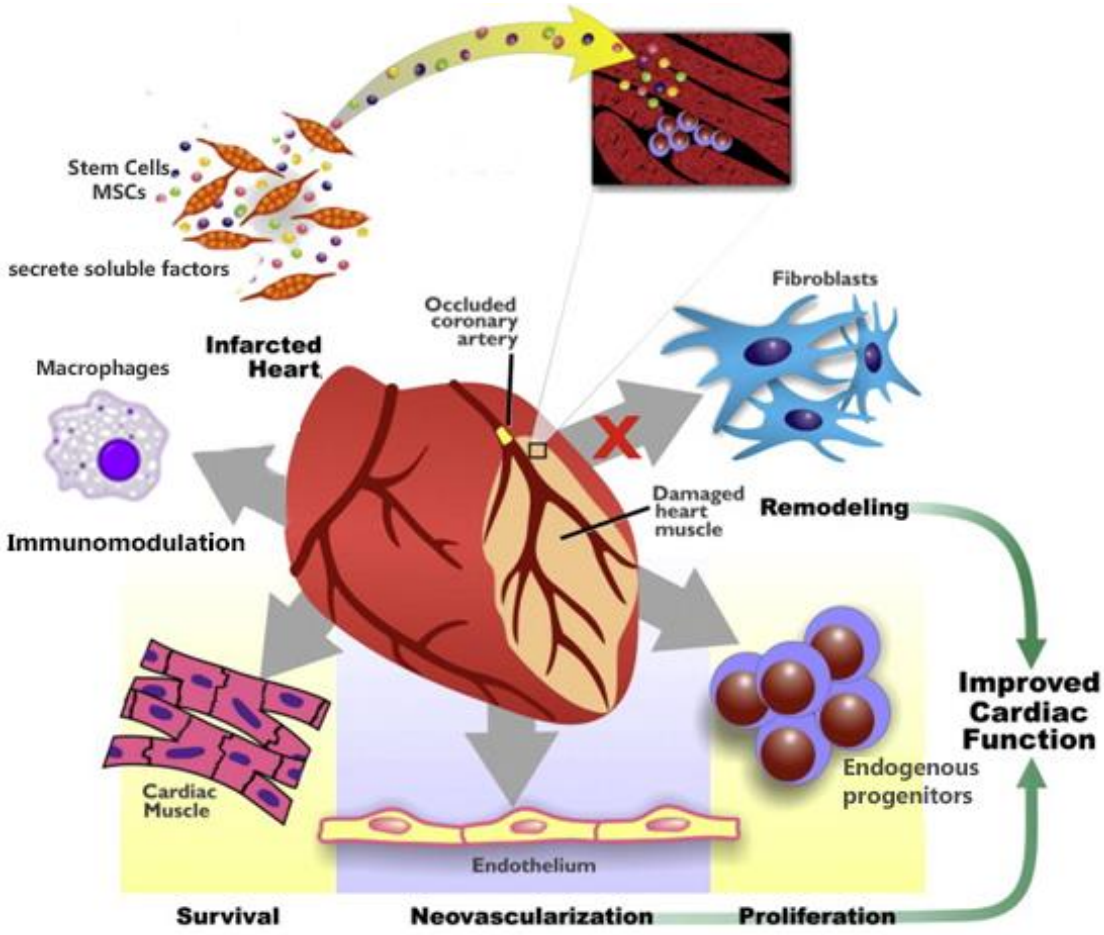

Figure 1 Schematic of paracrine activity on infarcted heart exerted by stem-mesenchymal stromal cell acting on macrophages, fibroblasts, cardiomyocytes, endothelial cells and endogenous cardiac progenitors. The outcome is an improved cardiac function. (adapted from: Mirotsou et Al. 2011[1])

From a translational clinical perspective, stimulation of cardiac tissue by paracrine therapy might represent an appealing approach to enhance cardiac repair following ischemic injury. Indeed, it provides a potential breakthrough in that, rather than administering cells, the specific content of the cell could be used, thus applying a cell-based, yet cell-free strategy for cardiac therapy. By doing so, many limiting aspects associated to canonical cell-therapy, such as poor cell engraftment and retention in the target tissue as well as immune rejection and technical limits could be overcome, while still ensuring beneficial effects.

1.2 The role of Extracellular Vesicles for paracrine therapy

In the context of the paracrine effects of stem cells, growing interest has recently been focused on the characterization of the vesicular counterpart of their secretome: the extracellular vesicles (EVs). The term EVs encompasses several subtypes of generated and expelled vesicles that are enclosed by a membrane bilayer containing bioactive molecules. The subtypes can be differentiated by their size, content, and route of intracellular formation (Figure 2)[25]:

- Exosomes (Exo) are very small vesicles (<200 nm), they are formed inside multivesicular bodies (MVB) within the endocytic pathway and are released in the extracellular space upon docking and fusion of MVB with cell plasma membrane,
- Microvesicles (MVs) are medium-sized vesicles (200–500 nm) formed by the outward budding and pinching of the cell plasma membrane
- Apoptotic bodies (>500 nm) result from the fractionation of the cellular content of cells undergoing programmed cell death[26].

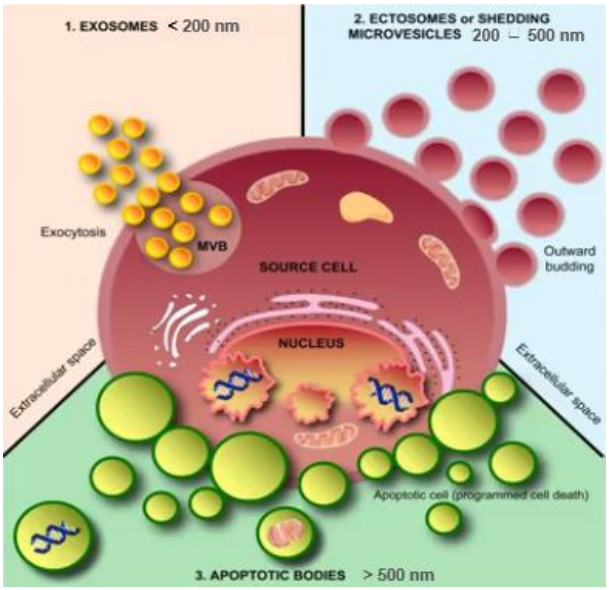

Figure 2. Schematic of extracellular vesicle fractions (adapted from Kalra et Al 2016[27])

EVs are enriched with different bioactive proteins, metabolites, biolipids and genetic information like RNA, (including messenger RNA (mRNA), but mostly long noncoding RNA (lncRNA) and microRNA (miRNA)), and harbour signalling molecules that target the behaviour of recipient cells. Several of these molecules are common among all EVs and others are specific of the EV-producing cells. Thus, they have recently emerged as critical paracrine conveyors of cell-to-cell information transfer in numerous biological systems[28] (Figure 3). In particular, EVs released by different types of stem/ progenitor cells have been investigated in various models of tissue injuries and have been shown to exert pro-regenerative effects through the modulation of relevant cellular processes such as proliferation, angiogenesis, oxidative stress, inflammation, and immunotolerance[26]. In the field of cardiovascular regeneration outstanding results have been obtained by EVs derived from mesenchymal stromal cells , as showing to decrease the infarct size in a murine model of heart-induced ischemia-reperfusion injury[29]; similar effects were observed from EVs derived by human umbilical cord MSCs (hUC-MSCs), protecting myocardial cells from apoptosis[26,30]. These results point towards a key role of secreted EVs in mediating cell-communication processes, as well as in acting as indirect paracrine mediators of delivered cells within host tissue following cell therapy[28,31]. The stem/progenitor - derived EVs may represent an appealing tool to be exploited for future paracrine therapy against cardiovascular disease and myocardial infarction. In this perspective, an ongoing quest is now focusing on defining the most ideal cell source for pro-regenerative EVs as characterized by relevant paracrine potential and significant self-renewal profile and feasibility of isolation.

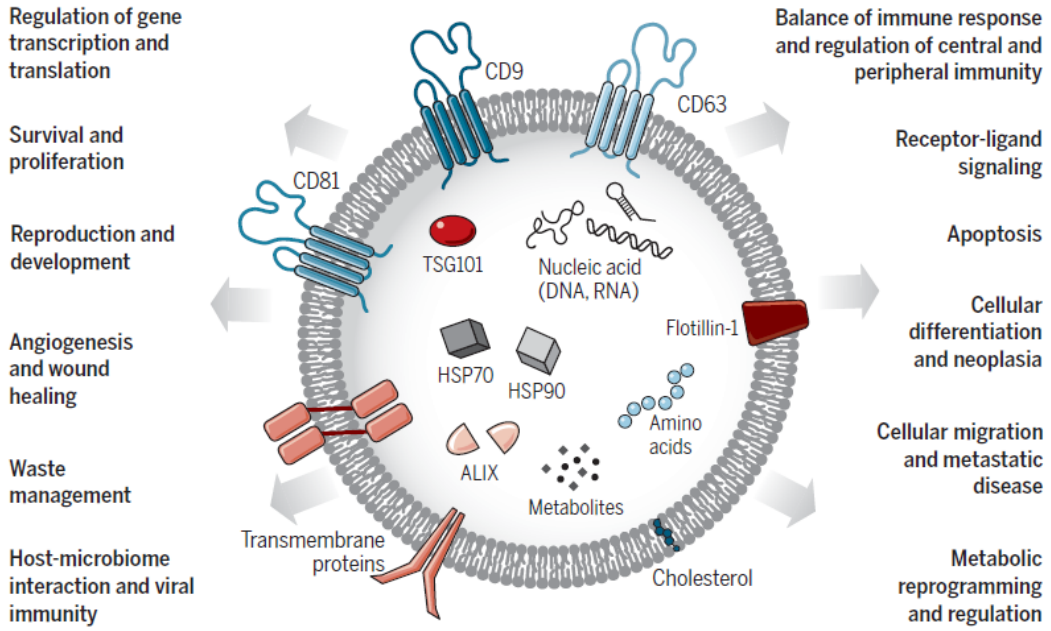

Figure 3. Schematic of the structure of small EV (also defined as exosome) and the main biological processes they can get involved during inter-cellular paracrine communication (from: Kalluri & LeBleu Science. 2020[32]).

1.3 Cardiovascular disease, cardiac repair and cardiac regeneration

The adult mammalian heart has been considered for long time an organ devoid of any regenerative potential with resident cardiomyocytes being post-mitotic and quiescent, hence made up of cells that do not renew themselves in the adult stage. Contrary to what occurs during embryonic and fetal cardiomyogenic development, in which the growth of the heart is mainly driven by active cardiomyocyte cell division (hyperplastic growth), in the postnatal period these cells stop proliferating and from this moment heart growth occurs essentially by hypertrophy[33,34]. Therefore, following severe injury – such as a myocardial infarction in which billions of resident contractile cardiomyocytes can be lost - the myocardium cannot regenerate via active renewal and proliferation of surviving cardiomyocytes and can only activate reparative pro-fibrotic mechanisms which almost appear as a failed paradigm of tissue regeneration.

Nonetheless, as demonstrated by Bergmann's group about 10 years ago, by means of a study based on the incorporation into living organisms of the ^{14}C carbon isotope in the atmosphere during nuclear bomb tests in the Cold War period, a small percentage of annual cardiac muscle tissue renewal is observable in the human heart, estimated at around 1% in adulthood, and further declines with increasing age[35]. Such limited endogenous regenerative capacity is clearly insufficient to compensate for the loss of functional cardiomyocytes following myocardial infarction; yet, this experimental evidence suggests that human endogenous regeneration mechanisms exist, although acting inefficiently and therefore they could be targeted and enhanced via therapeutic strategy.

However, it has been recently demonstrated that full cardiac regeneration via active cardiomyocyte renewal may occur in mammals, although strictly restricted to the period immediately following birth (Figure 4): indeed, it has been shown that neonatal mice, during a brief postnatal window of 7 days, can fully regenerate the heart through replacement of lost cardiomyocytes by new ones obtained by the surviving ones undergoing mitosis and cytokinesis. However, when cardiac injury happens in mice 7 days-old- or any older, the myocardium activates the canonical repair mechanism resulting in scarring and likely leading to the onset of heart failure during time (Figure 4)[36].

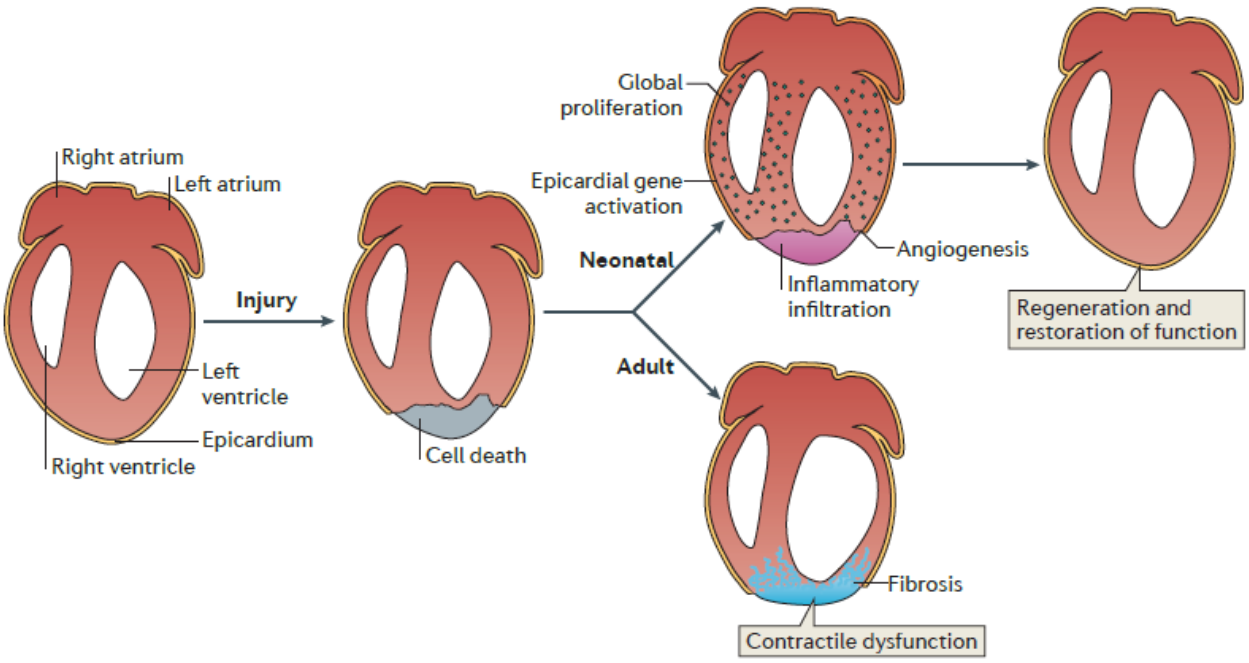

Figure 4 Schematic of cardiac regeneration in mouse during different developmental stages: neonatal period (till post-natal day 7) versus adulthood (from Xin, Olson and Bassel-Duby 2013 Nature Reviews[37])

All these evidences highlight the fact that cardiomyocytes may harbor endogenous proliferative capabilities, and that the adult cardiac tissue experiences a sort of "memory loss" affecting specific embryonic/early postnatal mechanisms, thus losing the regenerative potential during maturation into adulthood and maintaining only detrimental defective repair[28]. Myocardial renewal has become one of the major aims of cardiac regenerative medicine and preclinical research, having as objective the restoration of embrionic/post-natal mechanisms of cardiomyocytes proliferation after birth, with the idea of extending the neonatal regenerative window into adulthood. In this regard, paracrine stimulation using stem / progenitor cell secretome may represent an interesting strategy to restore the regenerative memory within cardiomyocytes in the injured myocardium.

1.4 Human stem cells derived from amniotic fluid as a valuable source of regenerative paracrine factors

Given the pivotal role that paracrine modulation has shown in different preclinical models of disease and in particular in those addressing myocardial infarction and/or cardiac damage, preclinical research is now focusing on identifying the most suitable stem/progenitor cell population endowed with the most cardio-active paracrine potential[28]. Therefore, it is important to find an optimal stem/progenitor cell source with feasible isolation and remarkable self-renewal potential. From this perspective, while adult somatic (e.g. bone marrow-mesenchymal stromal cells or BM-MSC) or embryonic stem cells may present limiting aspects, given their low yield, invasive sampling,

controversial self-renewal and ethical issues, mesenchymal stromal progenitors isolated from foetal and perinatal extra-embryonic tissues can offer an ideal alternative. Indeed, fetal and perinatal MSC can be easily obtained without ethical concerns from left over or discarded samples retrieved during prenatal diagnosis (i.e. amniocentesis or villi examination) or at term, after birth (i.e. placenta membranes and umbilical cord tissue). They show interesting *in vitro* proliferative potential, with a developmentally immature profile and with intermediate features between embryonic and adult somatic progenitors [38,39].

From this perspective, human amniotic fluid-derived stem cells (human Amniotic Fluid Stem cells-hAFS) represent a very appealing cell population. hAFS are multipotent mesenchymal progenitor cells, which can be easily isolated from a heterogeneous cell population derived from amniotic fluid waste samples obtained from amniocentesis for prenatal screening in pregnancy (II trimester) or at full term during scheduled caesarean delivery (III trimester) and selected for the expression of c-Kit (CD117), that is the type III tyrosine kinase receptor for stem cell factor with essential role in gametogenesis, melanogenesis and hematopoiesis[38,40] (Figure 5). This population was isolated for the first time by immunoselection in 2007 by De Coppi et al., and it counts for 1% of amniotic fluid cells population. c-kit+ hAFS present peculiar properties: they express a mesenchymal stromal cell phenotype, via the expression of classic markers including CD73, CD90, CD146 and CD105; they are endowed with remarkable self-renewal capability, clonogenesis, high doubling time (approx. 24-36h) and express pluripotency genes such as SSEA-4, and Nanog, thus resembling ES-like properties, but without being tumorigenic. They withstand cryopreservation for a long time while maintaining a stable karyotype[41], which makes their banking and scale up expansion very feasible[4].

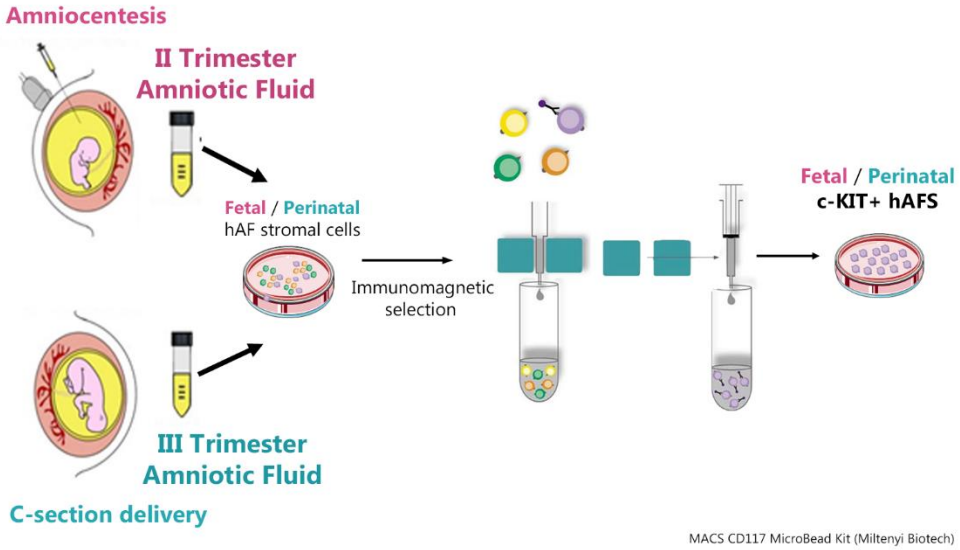

Figure 5 Schematic of c-KIT + hAFS isolation from amniotic fluid waste samples obtained by amniocentesis for prenatal screening in pregnancy (II trimester) or at full term during scheduled caesarean delivery (III trimester). hAF: human amniotic fluid.

In recent years hAFS have been described harbouring a remarkable cardioprotective paracrine profile, producing a secretome highly enriched with bioactive trophic factors, in which EVs show a notable regenerative profile.

Indeed, in a first study from 2011, the paracrine cardioprotective effect of hAFS cells was demonstrated by systemically injection into a rat preclinical model of acute myocardial infarction, obtained via ischemic injury and reperfusion (I/R). After ischemic induction, rats were treated either with hAFS cells or with their secretome, as the whole of soluble paracrine factors that cells released in their conditioned medium (hAFS-CM), resulting in a significant 14% reduction of the myocardial necrotic area with within 2 hours from systemic delivery administration. Considering the narrow time interval between cell administration and histological evaluation, such cardioprotective activity could be only referred to the paracrine effect exerted by the hAFS and mediated by the soluble factors within their hAFS-CM[10].

The paracrine potential of II trimester fetal hAFS was further validated in an *in vitro* model of cardiotoxicity on murine cardiomyocytes, subjected to the oncological pharmacological agent doxorubicin (Dox). Dox is a drug well-known to induce toxic side effects on cardiovascular cells when administered during chemotherapy[42]. The fetal hAFS-CM was demonstrated to antagonize in cardiomyocytes and in cardiac progenitor cells the premature senescence and apoptosis resulting from the noxious effects by Dox as causing DNA damage. In particular, since in the previous study it was observed that hAFS were activated in the ischemic environment and promoted cardiomyocyte survival in a paracrine manner, in this work a specific hypoxic preconditioning was optimized as a strategy to enrich hAFS-CM of cardioprotective factors by culturing secreting hAFS under 1% O_2 and in the absence of serum in the culture medium, i.e. under serum-free conditions. It was demonstrated that the hAFS-CM obtained by cells undergoing the hypoxic preconditioning induced the inhibition of the pro-senescent and pro-apoptotic effect on cardiomyocytes exposed to Dox via the positive modulation of two cardioprotective cytokines (IL-6 and CXCL-1) and the stimulation of the upstream intracellular signalling of NF-Kb and the PI3K/Akt pathway[4].

Recently, the functional biological profile of extracellular vesicles (EVs) isolated from the hAFS secretome (hAFS-CM) by serial ultracentrifugation (figure 6) has been also reported.

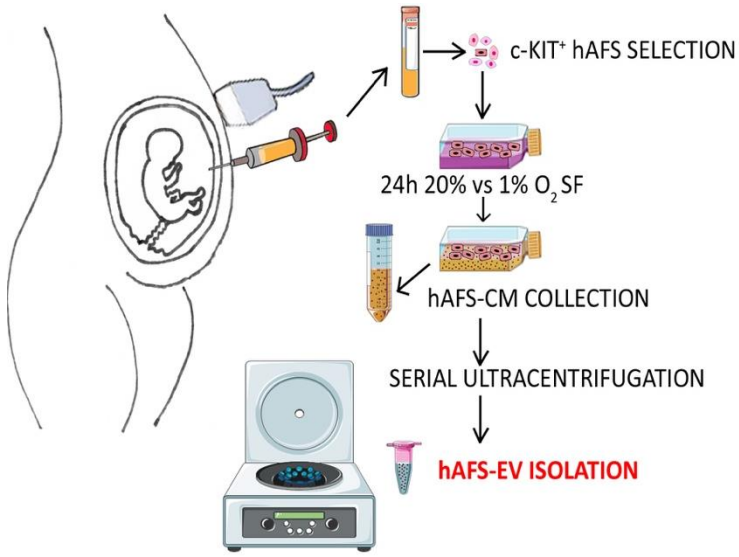

Figure 6. Schematic of hAFS-EV isolation as from Balbi et al. SCTM 2017 [3]

In particular, hAFS-EVs secreted by fetal hAFS undergoing hypoxic preconditioning showed high paracrine influence in mediating both proliferative and pro-survival effects on human fibroblasts and murine myoblast cells, while they expressed limited pro-angiogenic potential. Notably hAFS-EVs showed also relevant anti-inflammatory action when administered *in vivo* in a preclinical genetic model of skeletal muscular atrophy (Figure 7). The characterization of the microRNA content within the fetal hAFS-EV cargo showed enrichment with cardioprotective, anti-inflammatory and cardioactive markers (miR - 223, miR - 146a, miR - let7c, miR - 21, miR - 126, miR - 146b, miR - 199a - 3p, miR - 210) supporting the idea that paracrine effects mediated by hAFS-EV are attributable to a horizontal transfer in recipient cells of their contents of microRNA aimed to reprogram the target cell by modulating the already existing signaling pathways[3].

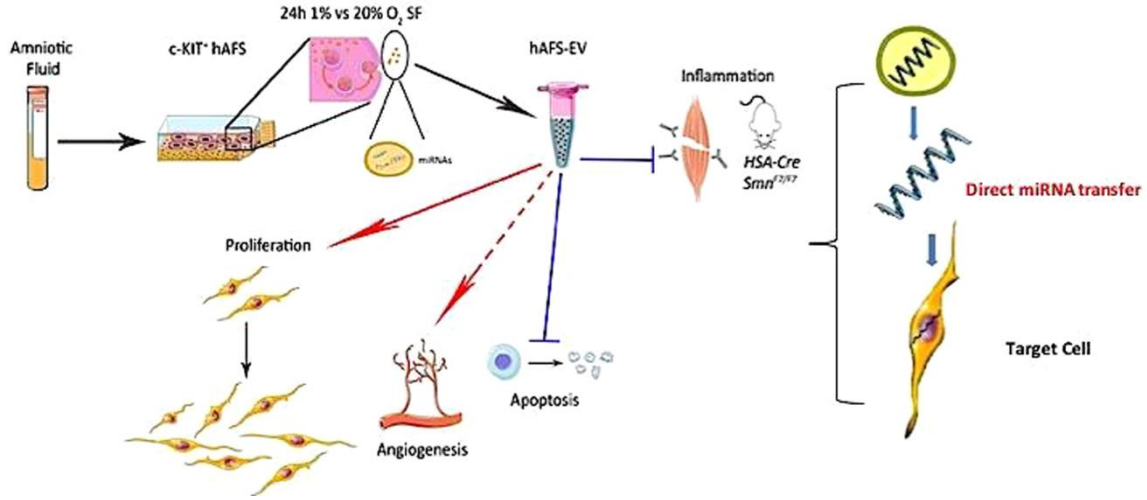

Figure 7. Paracrine effects of hAFS-EVs (from Balbi et al 2017[3])

The pro-regenerative effects of fetal hAFS-EVs have been further confirmed by independent work in the last years; indeed, several studies have recently focused on analysing the hAFS-EV paracrine profile against different pathological backgrounds of kidney disease, osteoarthritis, osteoporosis, necrotizing enterocolitis and neurodegenerative models with promising results[43–48].

In a more recent study, the potential of hAFS secretome fractions was analysed for cardiac regeneration, using a preclinical mouse model of acute myocardial infarction by permanent ligation of the coronary artery. In particular, hAFS-CM, hAFS-EVs and EVs-depleted hAFS-CM (hAFS-DM) were administered by inter-myocardial injection and compared for the long-term effects. However, of particular interest was the demonstration that hAFS-CM administered just once after MI reduced cardiac fibrosis, supported cardiac function and local angiogenesis, while stimulating endogenous cardiac progenitor cells from the epicardium (EPDC) and cardiomyocyte cell cycle progression in the long term, after 28 days. Moreover, hAFS-EVs alone were able to recapitulate all the beneficial effects exerted by hAFS-CM; indeed, recovery of cardiac function and possible influence on endogenous cardiomyocytes, was putatively attributable to the hAFS-EVs subfraction. On the contrary, as regards the modulation of local angiogenesis, the soluble fraction of the secretome (hAFS-CM) seemed to have a more marked modulatory capacity (Figure 8) [5].

.

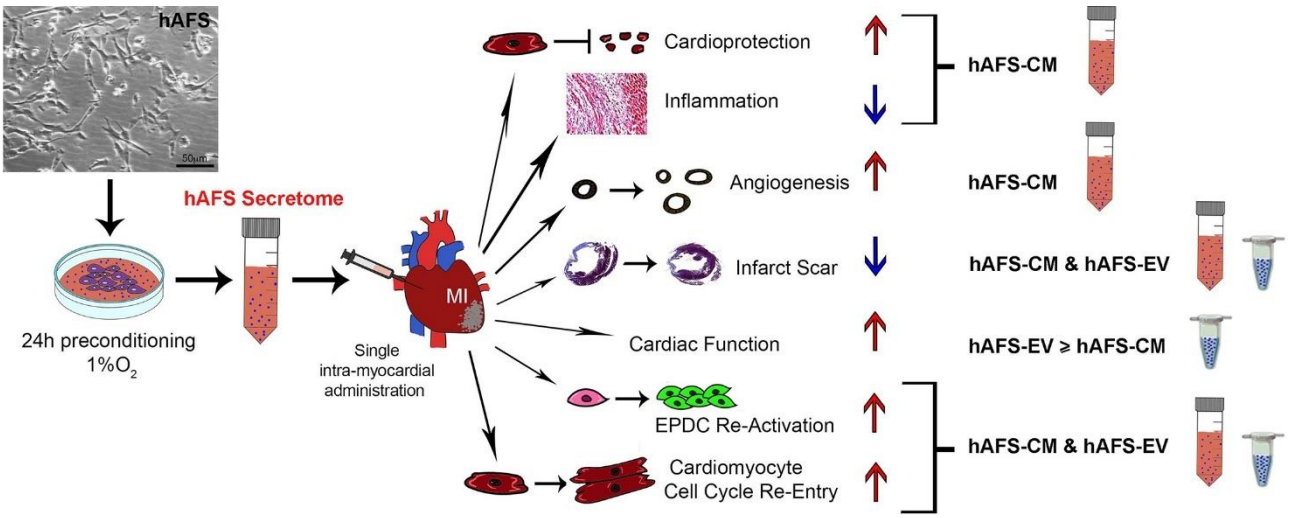

Figure 8. Cardio-active paracrine effects exerted by fetal hAFS-CM and hAFS-EVs in a preclinical mouse model of myocardial infarction (MI) as from Balbi et al. IJC 2019[5]. hAFS-EVs and hAFS-CM were effective in supporting cell cycle progression of cardiomyocytes.

1.5 From fetal to perinatal hAFS

The evidences previously reported support the possible future clinical translation of both total hAFS secretome (hAFS-CM) and hAFS-EVs for paracrine therapy, as the vesicular counterpart has showed a promising regenerative potential profile. However, most of these studies, that investigated the paracrine modulation of hAFS in the field of regenerative medicine, were performed with fetal hAFS, that is to say obtained by left-over samples by amniocentesis for prenatal screening.

Although amniotic fluid from II trimester still represents an important resource, from which hAFS could be selected, it is important that non-invasive prenatal testing (NIPT) has been recently developed to further protect the growing foetus/placenta during prenatal screening procedures[49].

As a consequence, the investigation of paracrine profile in perinatal hAFS, as obtained during III trimester from scheduled C-section amniotic fluid clinical waste, may be very interesting as alternative source of hAFS. Indeed, little is known about the regenerative capacity of III trimester perinatal hAFS: it has been demonstrated that they exert different immune regulatory properties compared to I- and II-trimester ones[50], while maintaining the ability to exert relevant endothelial regenerative potential[40] . Moreover, other perinatal sources such as umbilical-cord derived MSCs (UC-MSC), amniotic mesenchymal stromal cells (AMSC) have been reported to exert paracrine effects in preclinical animal models of myocardial injury, mainly resulting in modulation of local angiogenesis and ventricular remodelling[28,51–55].

Therefore, it would be relevant to further define the paracrine potential of perinatal (III trimester) human amniotic fluid progenitors compared to the fetal (II trimester) ones, so to suggest an ideal paracrine source for future cardiac regenerative medicine.

2 AIM OF THE STUDY

The aims of the study to which I contributed during my master thesis internship were the following:

- Define the cell gestational age influence on hAFS morphology, phenotype, and their metabolic activity by comparing II trimester fetal progenitors versus III trimester perinatal ones;
- Assess the role of hypoxic preconditioning effects in triggering fetal versus perinatal hAFS secretome yield in terms of both hAFS-CM and hAFS-EV formulations;
- Characterize in detail the fetal- and perinatal hAFS secretome fractions (hAFS-CM and hAFS-EVs) in terms of their protein, chemokine and cytokine content;
- Analyze the paracrine potential of fetal- and perinatal-hAFS secretome fractions in sustaining murine cardiomyocyte cell cycle re-entry and cell division *in vitro*.

All experimental procedures and analyses performed were designed and validated during my thesis internship in the research group coordinated by Prof. Sveva Bollini in the Regenerative Medicine Laboratory, Biology Unit, Department of Experimental Medicine, under the additional supervision of Dr. Ambra Costa, PhD student and Dr. Patrizia Garbati, Post Doc research fellow. Metabolic analyses on hAFS were performed under the supervision of Prof. Silvia Ravera from the Human Anatomy Unit, Department of Experimental Medicine.

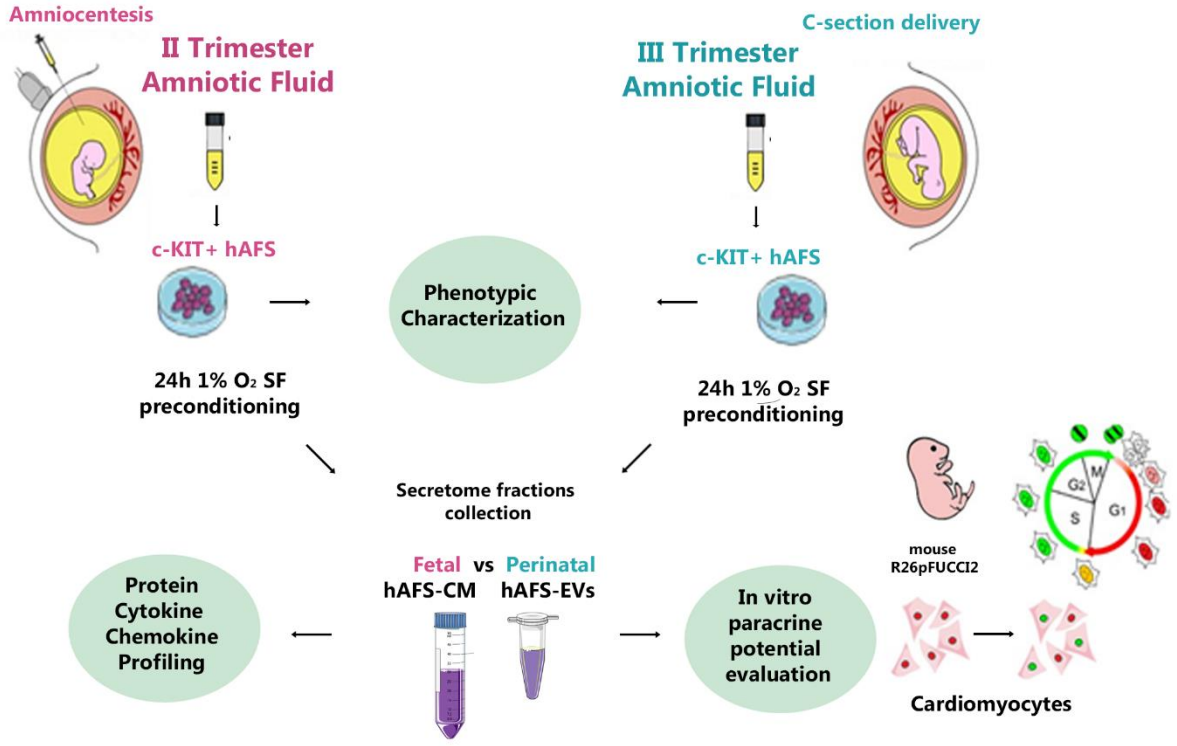

Figure 9 Schematic experimental design of the study

3 METHODS AND MATERIALS

3.1 In vitro human amniotic fluid-derived stem cell culture

3.1.1 Human amniotic fluid samples

Human amniotic fluid-derived stem cells (hAFS) were obtained from amniotic fluid (AF) samples as leftover specimens from II trimester prenatal diagnosis amniocenteses and from clinical waste of III trimester scheduled C-section delivery. Samples were obtained upon written informed consent of donors, from the Obstetrics and Gynaecology Unit, IRCCS San Martino Hospital and at the Fetal and Perinatal Medical and Surgery Unit and Human Genetics Laboratory at IRCCS Istituto Gaslini hospital (Genova, Italy). All procedures were performed in compliance with the Helsinki Declaration and following authorization by the Regional Ethical Committee (P.R. 428REG2015). II trimester fetal AF samples were obtained from female donors with average age of about 37.42±0.32 years old (n=15 ranging from 36- up to 41 years old); III trimester perinatal AF samples were obtained from female donors with average age of 34.25 ± 1.31 years old (n=10 ranging from 26- up to 42 years old).

3.1.2 Isolation and in vitro culture of hAFS

Fetal AF samples were centrifuged and cells resuspended and seeded in Chang Medium [10% Chang C and 88% Chang B (Irvine Scientific) supplemented with 1%glutamine, and 1% penicillin/streptomycin (Gibco-Thermo Fisher Scientific)] at 37°C with 5% CO_2 atmosphere. Perinatal AF samples were filtered by 70µm and 40µm filters; red blood cells were eliminated via incubation with Lysis Buffer (NH_4Cl 155 mM, $NaHCO_3$ 10 mM EDTA0.5 mM) for 10 min at room temperature. Samples were, then, centrifuged and cells seeded as for fetal AF samples.

After few days, nonadherent cells and debris were discarded and adherent stromal cells further cultivated up to the formation of single medium-sized colonies. hAFS were then immunomagnetically sorted from the adherent stromal cells upon c-Kit (CD117)[41] expression, by means of MACS CD117 MicroBead Kit following manufacturer's instructions (Miltenyi Biotech). c-Kit+ selected hAFS were grown in Minimal Essential Medium (MEM) alpha containing 15% FBS (Gibco-Thermo Fisher Scientific), 1% glutamine and 1% penicillin/streptomycin supplemented with 20% Chang Medium.

Fetal and perinatal hAFS (namely f-hAFS ans p-hAFS) were further cultured *in vitro* at 37 °C under 5% CO_2 atmosphere and maintained at sub-confluence (75%) until the fifth passage (P5), in which they were used to isolate their secretome.

3.2 Senescence staining

Cell senescence was evaluated by using the Senescence β-Galactosidase Staining Kit (Cell Signaling). The assay is based on the detection of senescence-associated β-galactosidase (SA-β-gal) activity, an enzyme that is overexpressed at pH 6.0 in aging cells differently from the acid β-galactosidase which is only detectable at pH 4.0. SA-βgal detection is revealed following incubation with the chromogenic substrate X-gal (5-bromo-4-chloro-3-indoyl-β-D-galactopiranoside). Xgal gets cleaved by β-galactosidase producing galactose and 5-bromo-4-chloro-3- hydroxindole. The latter is then oxidized into 5.5'-dibromo-4,4'-dichloro-indigo, an insoluble blue compound easily observable under an optical microscope[56].

f-hAFS and p-hAFS were fixed using a Fixative Solution 1X (diluted from a 10X solution made of 20% formaldehyde, 2% glutaraldehyde in PBS 10X) for 15 minutes at room temperature. After two PBS washes, the β-galactosidase Staining Solution was added to reveal β-gal activity. Cells were incubated at 37°C overnight, washed by PBS 1X solution. Images of senescent cells were acquired on a Leica DMi1 microscope (equipped with Leica Acquire software) and evaluated as percentage of SA-β-gal-positive cells over total cells per field.

3.3 Phenotypic characterization

The expression of mesenchymal stromal marker CD146 and of a lysosomal-associated membrane protein CD107a, previously associated with a highly secretory profile[57], was investigated in f-and p-hAFS by flow cytometry. 10^5 hAFS were detached by using Trypsin solution for 5 minutes, Trypsin was blocked with hAFS growing medium; cells then were centrifuged and washed with PBS 1X, then resuspended with 100 µl of 1X PBS and incubated for 15 min at 4°C with 2,5 µl of mouse anti-human-CD107a-Alexa Fluor 647-conjugated antibody and with the mouse anti-human-CD146-FITC-conjugated antibody (eBioscience). Events were acquired on a BD Bioscience FACS Aria II sorter and analyzer, equipped with FACS Diva software by Dr. Daniele Reverberi from Molecular Pathology Unit, IRCCS Ospedale Policlinico, San Martino, Genova, Italy. Data was analyzed using FlowJo V9.0 software (BD Bioscience).

3.4 Biochemical evaluation of hAFS metabolism

3.4.1 Oxygen consumption rate evaluation

O_2 consumption was evaluated using 10^5 fetal or perinatal hAFS, by an amperometric O_2 electrode in a closed chamber, magnetically stirred, at 37 °C (Unisense-Microrespiration, Unisense A/S, Denmark). Cells were permeabilized for 5 min with 0.03% digitonin and resuspended in PBS 1X. The addition of the respiring substrates was performed with a Hamilton syringe in the following order: 10 mM pyruvate plus 5 mM malate, and 20 mM succinate. Pyruvate and malate were used to stimulate the pathway composed by Complexes I, III and IV, while succinate was used for the pathway formed by Complexes II, III and IV.

Evaluation of O_2 consumption was also performed mimicking a Seahorse kit (Seahorse XF Mito Fuel Flex Test Kit - Agilent) in order to evaluate the relative contributions of glutamine, long-chain fatty acids and glucose to respiration. In this case, before each experiment, the electrode was equilibrated with the growing medium, in which the oxygen consumption rate (OCR) was evaluated. Cells were permeabilized for 5 min with 0.03% digitonin and resuspended in their growing medium. 5 µM of three different metabolism inhibitors were added with a Hamilton syringe in the following order:

- BPTES (bis-2-(5-phenylacetamido-1,3,4-thiadiazol-2-yl) ethyl sulfide), an allosteric and selective glutaminase inhibitor
- Etomoxir, an irreversible inhibitor of carnitine palmitoyltransferase-1A (CPT1A) on the inner face of the outer mitochondrial membrane
- UK5099 (acyano-(1-phenylindol-3-yl)-acrylate), an inhibitor of mitochondrial pyruvate carrier (MPC)

The respiratory rates were expressed as nmol O/min/10^6 cells.

3.4.2 Evaluation of ATP synthesis

F1Fo-ATP synthase (ATP synthase) activity was detected by measuring the ATP production through a highly sensitive luciferin/luciferase chemiluminescent method. This method uses the ATP dependency of the light-emitting luciferase-catalysed oxidation of luciferin for the measurement of extremely low ATP concentrations:

$$\text{ATP} + \text{D-luciferin} + \text{O}_2 \xrightarrow{\text{Luciferase}} \text{oxyluciferin} + \text{PPi} + \text{AMP} + \text{CO}_2 + \text{light}$$

The resulting green light has an emission maximum at 562 nm and can be detected by a luminometer and measured in RLU (Relative Light Unit).

10^5 of f- and p-hAFS cells were incubated for 10 min at 37°C in a medium containing: 50 mM KCl, 1 mM EGTA, 2 mM EDTA, 5 mM KH_2PO_4, 2 mM $MgCl_2$, 0.6 mM ouabain, 1 mM P1P5-Di(adenosine-5) penta- phosphate, 0.040 mg/ml ampicillin, and 10mM Tris-HCl pH7.4 (Carlo Erba Reagents). Afterward, ATP synthesis was evaluated by the addition of 10mM pyruvate plus 5 mM malate or 20 mM succinate (inducing substrates) and to initiate the reaction 100 µl of Luciferin/Luciferase were added in 100 µl of sample solution, together with 0,1 mM ADP. The reaction was monitored for 2 minutes, every 30 s, in a luminometer (GloMax® 20/20n Luminometer, Promega Italia, Milano, Italy). ATP standard solutions in the concentration range of 10^{-10}-10^{-7} M were used for the calibration (luciferin/luciferase ATP bioluminescence assay kit CLSII, Roche, Basel, Switzerland).

When the ATP synthesis was assessed in presence of 5 µM BPTES, 5 µM Etomoxir or 5 µM UK5099, 10^5 cells were incubated for 10 min in the growth medium in the absence or presence of one of the metabolism inhibitors, then the procedure was as previously described. Data were expressed as nmol ATP produced/min/10^6 cells.

3.4.3 Evaluation of P/O ratio

The P/O ratio refers to the number of phosphates that are fixed into ATP for every two electrons that pass from a substrate to reduce each oxygen atom of molecular O_2. Hence, it is a good indicator of a coupled status between electron transport chain and ATP synthase, that's to say an indicator of the OxPhos (oxidative phosphorylation) efficiency. Experimentally it has been shown that the protons pumped out of the mitochondrion for each pair of electrons are 10 for the NADH linked substrate (e.g. pyruvate + malate) and 6 for succinate; as 4 H^+ are needed for the synthesis of an ATP (one of which is needed to transport Pi, ADP and ATP across the mitochondrial membrane), the P/O ratio is equal to 2.5 (10/4) for NADH and 1.5 (6/4) for the $FADH_2$ linked substrate (e.g. succinate)[58].

The P/O ratio was evaluated as the ratio between the nmol of synthesized ATP, detected by luminometry and the nmol of O consumed, in the presence of metabolism inhibitors (BPTES, Etomoxir, UK5099) or of the chosen respiring substrates (pyruvate/malate and succinate).

3.4.4 Evaluation of glucose consumption

To evaluate the contribution of anaerobic glycolysis to the hAFS metabolism, glucose and lactate concentrations were evaluated in the growth medium.

The glucose concentration was evaluated in the growth medium of f- and p-hAFS by the spectrophotometric measurement of NADPH at λ=340 nm, obtained from the following reactions:

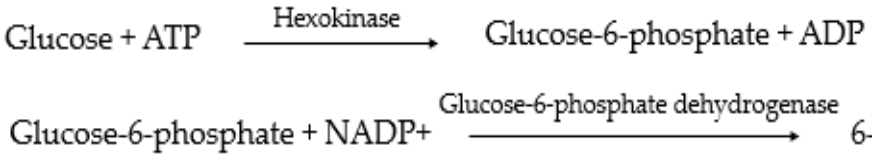

The assay mixture contained: 100mM Tris–HCl pH 7.4, 2 mM $MgCl_2$, 0,5 mM NADP, 1 mM ATP and 4 µg/ml of purified hexokinase (HK) + glucose-6-phosphate dehydrogenase (G6PDH). Samples were analysed spectrophotometrically before and after the addition of 1 µl of HK + G6PDH. Data were normalized on the cell number.

3.4.5 Evaluation of lactate release

The lactate concentration was evaluated in the growth medium of fetal and perinatal hAFS by the spectrophotometric measurement of NADH at λ=340 nm, obtained from the following reaction:

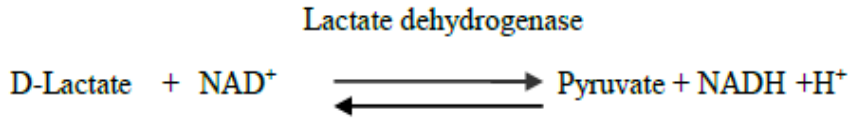

.

The assay mixture contained 100mM Tris–HCl pH 9, 5 mM NAD+ and 4 µg of lactate dehydrogenase (LDH). Samples were analysed spectrophotometrically before and after the addition of 1 µl of purified LDH. Data were normalized on the cell number.

Anaerobic glycolysis yield was evaluated by the ratio of the released lactate and the theoretical lactate production. This last value is obtained considering that 2 molecules of pyruvate are produced by 1 molecule of glucose; in conditions of only anaerobic metabolism all the pyruvate can be used for fermentation to produce 2 molecules of lactate. Thus, theoretical lactate production can be calculated as two-fold of glucose consumption.

3.5 Hypoxic preconditioning of hAFS

f-hAFS and p-hAFS were cultured in normoxic or hypoxic conditions for 24h in serum-free medium (SF) as preconditioning strategy to improve the release of bio-active paracrine factors, as previously reported by Prof. Bollini's team[3–5].

hAFS were cultured up to 70%–80% confluency until P5 and subsequently washed with 1X PBS solution to be then incubated for 30 min with SF medium (high glucose Dulbecco's Modified Eagle's Medium - DMEM, with 1% L-glutamine and 1% penicillin/streptomycin, all from Gibco-Thermo Fisher Scientific), in order to remove all FBS and Chang components. f- and p-hAFS were then cultured for 24h in SF medium under control normoxic (20% O_2 and 5% CO_2 atmosphere at 37°C in a standard CellXpert® C170i incubator, Eppendorf) versus hypoxic condition (1% O_2 and 5% CO_2 at 37°C in a Galaxy® 48R incubator, Eppendorf).

3.6 Apoptotic assay

f-hAFS and p-hAFS viability after 24h preconditioning culture setting was evaluated by flow cytometry with the Annexin V-AF647/PI Apoptosis Detection Kit (Elabscience). Early apoptotic cells are characterized by translocation of phospholipid phosphatidylserine (PS) from the inner to the outer leaflet of the intact plasma membrane; they are positive for Annexin V, a Ca^{2+}-dependent binding protein with high affinity, specificity, and sensitivity for PS. Late apoptotic cell plasma membrane, becomes permeable to Propidium Iodide (PI), a dye that when bound to DNA increases the fluorescence signal by nearly 20-fold.

10^5 f- and p-hAFS were detached and incubated in 500 µl of 1X Annexin V Binding Buffer with 5 µl of Annexin V-AF647 and 5 µl of Propidium Iodide (PI) solution. After the incubation at room temperature for 15-20 min in the dark, events were acquired on a BD Bioscience FACS Aria II sorter and analyzer, with FACS Diva software by Dr. Daniele Reverberi from Molecular Pathology Unit, IRCCS Ospedale Policlinico, San Martino, Genova, Italy. Data was analysed using FlowJo V9.0 software (BD Bioscience).

3.7 Separation and concentration of hAFS secretome fractions

Cell-conditioned medium was collected from f-hAFS (f-hAFS-CM) and p-hAFS (p-hAFS-CM) undergoing 24h preconditioning *in vitro* and centrifuged at 4°C at 300×g for 10' and 2000×g for 20' to remove cell debris; hAFS-CM was first concentrated using ultrafiltration membranes with a 3 kDa

selective cut-off (Amicon Ultra-15, Millipore, Burlington, Massachusetts) at 4°C at 3000×g for 90' and then further concentrated at 4°C at 3000×g for 30', reaching at least a concentration of ca. 20X.

Fetal- and perinatal hAFS-EVs (f-hAFS-EVs and p-hAFS-EVs, respectively) were separated from hAFS-CM by serial ultracentrifugation from concentrated hAFS-CM. hAFS-CM was collected and centrifuged at 4°C at 300×g for 10', 2000×g for 20' to remove cell debris. Supernatant was then processed at 10,000×g for 40'. Pellet was then discarded and supernatant further processed by ultracentrifugation in an Optima L-90K (Beckmann Coulter, Brea, California) at 100,000×g for 120' using Beckman Coulter's swinging-bucket SW55Ti or SW44Ti centrifuge rotors. The pellet containing heterogenous hAFS-EVs was washed in PBS by a final step at 100,000×g for 120' and then resuspended in ca. 40 µl of 0.22 µm filtered PBS. hAFS-CM and hAFS-EV protein concentration was measured using the BiCinchoninic Acid (BCA) assay (Thermo Fisher Scientific, Waltham, Massachusetts). The BCA test is based on a colorimetric reaction by which the colour of the sample solution changes from green to purple in proportion to the concentration of proteins. This is possible because peptide bonds in proteins reduce Cu^{2+} ions from copper (II) sulfate to Cu^{+}; each Cu^{+} ion can be chelated by two molecules of bicinchoninic acid, forming a purple-coloured complex that strongly absorbs light at a wavelength of 562 nm; Cu+ complex formation, however, is influenced by the presence of cysteine/cystine, tyrosine, and tryptophan side chains. The absorption maintains a direct proportionality in a concentration range of 20-2000 µg/ml. Since the BCA method is not a true end-point method, protein concentrations were always determined in relation to a calibration curve using BSA (bovine serum albumin), as protein standard. A standard curve with a range of 5-250 µg/ml (micro-curve) was used for hAFS-EVs, while a standard curve of 20-2000 µg/ml (macro-curve) was used for hAFS-CM. hAFS-CM samples and macro-curve standards were incubated at 37°C for 45 min, while hAFS-EVs samples and micro-curve standards were incubated at 60°C for 30 min; the reaction was then blocked in ice. The higher temperature for the micro-curve is recommended in order to increase assay sensitivity, while minimizing the variances caused by unequal amino acid composition.

For the analyses hAFS-CM samples were diluted 1:5 in PBS, and in DMEM solution diluted 1:5 in PBS was used as blank reference. hAFS-EVs samples were not diluted and 0.22 µm filtered PBS was used as blank reference. Samples were acquired on a Gen5 Microplate Reader at wavelength 570nm to calculate hAFS-CM and hAFS-EV yield in terms of µg of solution/10^6 producing cells.

3.8 Characterization of hAFS-EVs by transmission electron microscopy and Nanoparticle Tracking Analysis

Transmission electron microscopy (TEM) analysis and data interpretation were carried out in collaboration with Prof. Katia Cortese and Dr. Sara Santamaria from the Human Anatomy Unit, Department of Experimental Medicine (DIMES), University of Genova. Data acquisition was performed on a Hitachi TEM microscope (HT7800 series). Digital images were taken with a Megaview 3 camera and Radius software (EMSIS). f-hAFS and p-hAFS were fixed in 3.7% paraformaldehyde (PFA) solution diluted 1:1 with hAFS complete medium, washed out in 0.1M cacodylate buffer and then immediately incubated in 0.1M cacodylate buffer containing 2.5% glutaraldehyde (Electron Microscopy Science), for 1h at room temperature. Cells pellets were post-fixed in osmium tetroxide for 2h and in a 1% uranyl acetate solution for 1 h. Samples were dehydrated through a graded ethanol series and embedded in epoxy resin (Poly-Bed; Polysciences) for 24 h at 60°C. Ultrathin sections (50 nm) were cut with Leica Ultracut microtome and stained with a 5% uranyl acetate in 50% ethanol solution.

f-hAFS-EVs and p-hAFS-EVs were resuspended in 20µL PBS solution and fixed by adding an equal volume of 2% paraformaldehyde in 0.1M phosphate buffer solution (pH 7.4). EVs were then adsorbed for 10 minutes onto formvar-carbon coated copper grids by floating the grids on 5µl drops on parafilm. Subsequently, grids with adhering EVs were rinsed in PBS and negatively stained by 2% uranyl acetate solution for 5 minutes at room temperature. Stained grids were embedded in 2.5% methylcellulose for improved preservation and air dried before examination. Morphometry analysis of hAFS-EVs was measured on 10 randomly taken micrographs at 40.000x magnification. Size was calculated using the arbitrary line function embedded in the measurement dialog box of Radius software (EMSIS). To visualize hAFS-EV size distribution, results were plotted as scatter dot plot and as frequency distribution, in which each size measure is represented as a point along with lines for the median value and the range.

f-hAFS-EVs and p-hAFS-EVs were also analyzed by Nanoparticle Tracking Analysis (NTA) with the help of Dr. Carolina Balbi from the Laboratory of Cellular and Molecular Cardiology, Cardiocentro Ticino Foundation, Lugano, Switzerland, in order to assess particles released by 10^6 cells. hAFS-EVs were diluted 1:1000 in PBS solution and acquired on a NanoSight LM10 (Malvern Instruments, Malvern), recording at least 3 different frames of 60s each. Three different acquisitions for each sample were analyzed using the Batch Process option in the software.

3.9 Comparative proteomic evaluation of hAFS-CM and hAFS-EVs and data analysis

Proteomics analysis was performed in collaboration with Dr. Antonella De Palma and Dr. Pierluigi Mauri from the Proteomics and Metabolomics Unit, Institute for Biomedical Technologies (ITB-CNR), Milan, Italy, who also assisted for data interpretation.

hAFS-CM and hAFS-EV samples were resuspended in 0.1M NH_4HCO_3 pH 7.9 and treated with RapigestTM SF reagent (Waters Co.). The resulting suspensions were incubated under stirring at 100°C for 20 minutes. The digestion was carried out on each sample by serial adding Sequencing Grade Modified Trypsin (Promega Inc.) Moreover, the addition of 0.5% Trifluoroacetic acid (TFA, Sigma-Aldrich Inc.) stopped the enzymatic reaction, and a subsequent incubation at 37 °C for 45 min completed the RapiGest acid hydrolysis Finally, the tryptic digest mixtures were desalted using PierceTM C-18 spin columns (Thermo Fisher Scientific - Pierce Biotechnology), according to manufacturer protocol and resuspended in 0.1% formic acid (Sigma-Aldrich) in water (LC-MS Ultra CHROMASOLV™, Honeywell Riedel-de HaenTM). Mass Spectrometry analyses were performed on LTQ-OrbitrapXL mass spectrometer (Thermo Fisher Scientific) equipped with a nanospray ion source. Mass spectrometer scan functions and high-performance liquid chromatography solvent gradients were controlled by the Xcalibur data system version 1.4 (Thermo Fisher).

All generated data were searched using the Sequest HT search engine contained in the Thermo Scientific Proteome Discoverer software, version 2.1. The experimental MS/MS spectra were correlated to tryptic peptide sequences by comparison with the theoretical mass spectra obtained by in silico digestion of the Uniprot Homo Sapiens proteome database (74600 entries), downloaded in January 2020 (www.uniprot.org). Percolator node was used with a target-decoy strategy to give a final false discovery rates (FDR) at Peptide Spectrum Match (PSM) level of 0.01 (strict) based on q-values, considering maximum delta CN of 0.05. Only peptides with minimum peptide length of six amino acids and rank 1 were considered. Protein grouping and strict parsimony principle were applied. To select differentially expressed proteins, subgroups (for both fetal- vs perinatal- hAFS-CM and hAFS-EVs, considering also hypoxic cell preconditioning stimulation) were pairwise compared, applying a threshold of 0.4 and 5 on the two MAProMa indexes DAve (Differential Average) and DCI (Differential Confidence Index), respectively.

3.10 Cytokine and chemokine profiling of hAFS-CM and hAFS-EVs

Cytokine and chemokine profiling of hAFS-CM and hAFS-EVs obtained by f-hAFS and p-hAFS undergoing hypoxic preconditioning was assessed by means of Proteome Pro-filer™ Human XL Cytokine Array kit (R&D System, Minnesota, US) according to manufacturer's instructions. 20 µg of hAFS-CM and hAFS-EV sample was used. Membranes images were acquired by a Chemidoc Mini HD9 Auto (Uvitec Cambridge). Specific cytokine/chemokine content was evaluated by the quantification of positive pixel intensity (by means of arbitrary unit) for each detectable cytokine by ImageJ software (https://imagej.nih.gov/ij/).

3.11 In vitro primary culture of murine cardiomyocytes

3.11.1 R26pFUCCI2 mouse model for cell cycle fluorescent labelling

Murine cardiomyocytes were isolated from the neonatal cardiac tissue of heterozygous transgenic R26pFUCCI2 (Fluorescence Ubiquitination-based Cell Cycle Indicator) mice. The R26pFUCCI2 mouse model carries a single transgene probe system targeting specific cell-cycle regulating proteins by alternative nuclear fluorescent signals[59]. A pair of fluorescent proteins are fused to the Cdt1 and Geminin proteins, which expression oscillates during the cell cycle with an inverse pattern: Cdt1 protein peaks in G1 phase, while Geminin levels are high during S/G2/M phase. Nuclear Cdt1 expression is labelled by mCherry signals [mCherry-hCdt1(30/120), detected in red], while Geminin is marked by mVenus fluorescence [mVenus-hGem(1/110), as detected in green]; they are bidirectionally directed by Rosa26 promoter (R26p), allowing fluorescent nuclear labelling according to cell cycle stage (Figure 10). Transgenic R26pFUCCI2 mice were obtained via an MTA agreement [CDB0203T] from RIKEN Center for Life Science technologies, Kobe Japan. R26pFUCCI2 mouse colony was maintained by crossing R26pFUCCI2 heterozygous mice with C57Bl6/J female wild type mice. Mice were housed and maintained in the IRCCS San Martino Hospital Animal facility in compliance with national and European international standards of animal care and according to required authorisation from the Italian Ministry of Health (authorization n. 62/2019-PR from Italian Ministry of Health) to Prof. Bollini. Transgenic heterozygous R26pFUCCI2 mice were determined by genotyping analysis of ear biopsies on mouse pups. Tissue samples were digested and genomic DNA isolated via Phire Tissue Direct PCR Master Mix (Thermo Scientific) according to manufacturer's instructions. Genomic PCR analysis was performed using the following RNA primers designed for detecting the presence of the mVenus gene (5′-ATG GTG AGC AAG GGC GAG GAG-

3′ and 5′-CTT GTA CAG CTC GTC CAT GCC G-3′). PCR products were analyzed by gel electrophoresis: 10 µl of PCR samples were loaded and run for 15 minutes at 100 V on a 2% agarose gel in 1X TBE buffer (Tris-borate-EDTA) containing 1:10000 diluted Sybr Safe for DNA staining. To verify the presence of the amplified gene the gel was placed under UV light and checked for mVenus corresponding band.

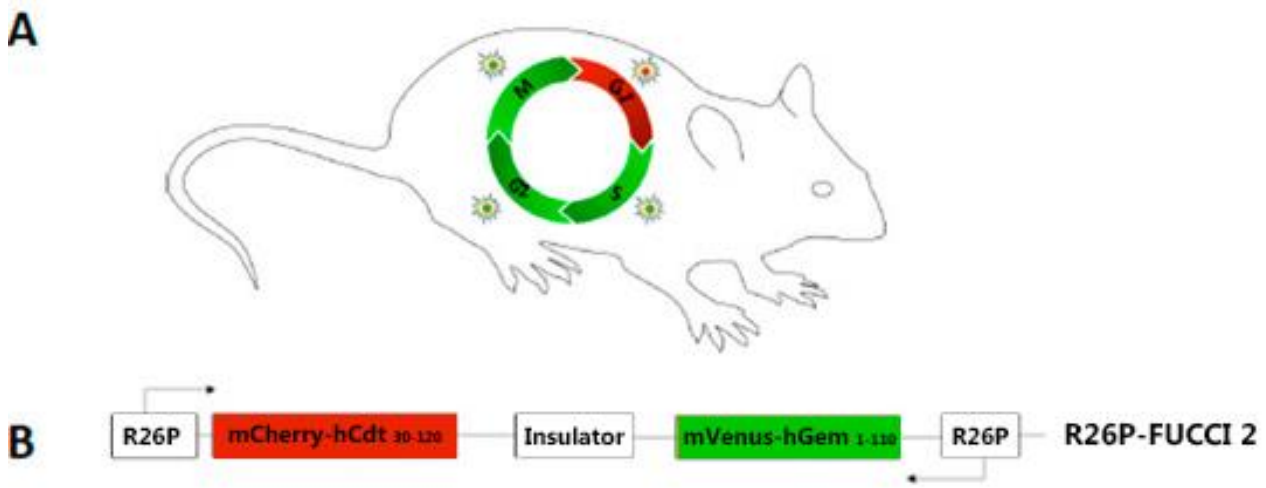

Figure 10 Schematic of the single transgene construct probe system (B) carried by R26pFUCCI2 mouse model, targeting specific cell-cycle regulating proteins by alternative nuclear fluorescent signals (A) (adapted from Preston et al. May 2018, Int J of Mol Sci[60])

3.11.2 Primary culture of neonatal mouse ventricular cardiomyocytes

Neonatal mouse ventricular cardiomyocytes (mNVCM) were obtained from mouse pups obtained from the crossing of male transgenic R26pFUCCI2 heterozygous mice with female wild type FVB mice, according to authorisation from the Italian Ministry of Health (authorization n. 62/2019-PR from Italian Ministry of Health). mNVCM were isolated via enzymatic digestion of the mouse neonatal cardiac tissue using the Pierce Primary Cardiomyocyte Isolation Kit (Thermo Scientific). 1-day-old R26pFUCCI2 mouse pup hearts were placed in 1.5 ml sterile tubes with ice cold HBSS (Hanks'Balanced Salt Solution without $Ca^{2+/}Mg^{2+)}$ and minced into 1-3 mm^3 pieces; samples were then washed twice in cold HBSS in order to remove blood. 0.2 ml reconstituted Cardiomyocyte Isolation Enzyme 1 (with papain) and 10µl Cardiomyocyte Isolation Enzyme 2 (with thermolysin) were added to each sample and incubated at 37°C for 30-35 minutes to allow enzymatic digestion of tissue fragments. Enzyme solution was then removed and tissue washed twice with HBSS. Tissue remnants were eventually dissolved in solution by gently pipetting. Cell solution was centrifuged, the cell pellet resuspended in complete cardiomyocyte culture medium (DMEM with 10% heat-

inactivated fetal bovine serum (FBS) with1% Penicillin-streptomycin) and counted via trypan blue viability dye staining. mNVCM were seeded on 0.2% gelatin (Sigma-Aldrich) and fibronectin (1:1000 diluted solution) coated 8-well PCA detachable chamber slide (SARSTEDT, Germany) at 10^5 cells/cm^2.

3.12 In vitro stimulation of R26pFUCCI2+/- mNVCM by fetal versus perinatal hAFS-CM and hAFS-EVs, and immunostaining analysis

Two days after seeding, mNVCM were treated with 80 μg/ml fetal or perinatal hAFS-CM (as previously determined as working concentration in[3]) or with 1 μg/well fetal or perinatal hAFS-EVs, all obtained from hAFS undergoing hypoxic preconditioning, for further 48h in serum free medium. As negative comparative control, mNVCM incubated with DMEM serum free solution were used. mNVCM cell cycle progression was then evaluated 72h after treatment by monitoring the switching from nuclear red mCherry fluorescent signal (G0 phase) to the green mVenus one (S-G2-M phase) in cells co-expressing a sarcomeric marker, i.e. sarcomeric alpha-actinin (αAct), by fluorescent immunostaining technique. mNVCM were fixed in 3.7% paraformaldehyde solution (Sigma Aldrich) for 10 minutes at room temperature, washed twice with PBS and permeabilized with 0.25% Triton solution for 5 minutes. Blocking solution [3% BSA in PBST (0,25% Triton in PBS 1X)] was added to the cells for 1 hour to avoid unspecific binding of antibodies. mNVCM were incubated overnight at 4°C with the following primary antibodies diluted in 1,5% BSA in PBST: chicken monoclonal antibody anti-GFP (ab13970, Abcam, Cambridge, UK), used to enhance the endogenous mVenus probe nuclear signal; mouse monoclonal antibody anti-sarcomeric alpha actinin (αAct, ab9465, Abcam, Cambridge, UK); rabbit monoclonal antibody anti-Aurora B kinase (a chromosomal passenger protein involved in the cleavage furrow and midbodies, thus marking cytokinesis, AuBK, ab2254, Abcam, Cambridge, UK). After 3 washes for 5 minutes each, the following secondary antibodies were incubated for 1,5h at room temperature: anti-chicken Alexa Fluor488-conjugated secondary antibody (A-11039, Thermo Fisher Scientific), anti-mouse Alexa Fluor594-conjugated secondary antibody (A-11032, Thermo Fisher Scientific), and anti-rabbit Alexa Fluor647-conjugated secondary antibody (A-32733, Thermo Fisher Scientific). After 3 washes, DAPI - 4′,6-diamidino-2-phenylindole – (Thermo Fisher Scientific) was added to stain cell nuclei. Immunostaining images were acquired with an Axiovert microscope equipped with Axiovision software (Carl Zeiss). The fetal versus perinatal hAFS-CM and hAFS-EV potential to support cardiomyocyte cell cycle progression was assessed as the percentage of αAct-positive mNVCM expressing nuclear mVenus signal enhanced via anti-GFP antibody over the total αAct-positive mNVCM per field. Cytokinesis

events were detected as the percentage of αAct-positive mNVCM expressing Aurora B kinase localizing at the midbody (Figure 11).

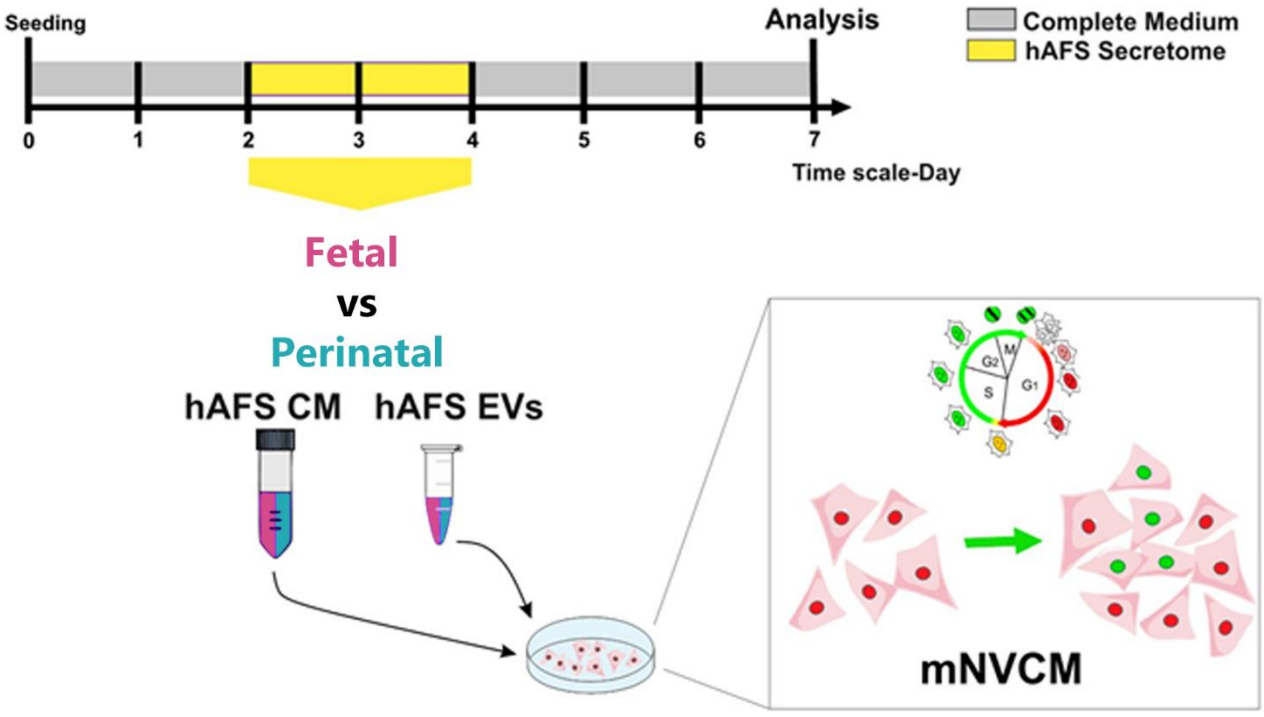

Figure 11 Schematic of *in vitro* mNVCM stimulation with hAFS secretome fractions (hAFS-CM or hAFS-EVs) and cell-cycle progression analysis.

3.13 Statistical analysis

Results are presented as mean ± s.e.m of at least three (n=3) independent replicated experiments. Comparisons were drawn by one-way ANOVA followed by post-hoc Tukey's multiple comparisons test or by Student t-test. Analyses were performed using Graph-Pad Prism Version 8.0.2 (GraphPad Software) with statistical significance set at *$p<0.05$. For proteomics analysis, the distribution of proteins in the examined conditions was achieved using FunRich (version 3.1.3, http://www.funrich.org/) that uses hypergeometric test and bonferroni for statistics and allows the graphical visualization of data with bar charts.

4 RESULTS

4.1 Perinatal hAFS show a close phenotypic match to fetal hAFS

Fetal c-KIT$^+$ hAFS (f-hAFS, as obtained from II trimester amniotic fluid samples) and perinatal c-KIT$^+$ hAFS (p-hAFS, isolated from III trimester amniotic fluid clinical waste), confirmed similar phenotypic features with heterogeneous morphology, as previously reported [40,41] (Figure 12)**.** Both f-hAFS and p-hAFS cultured *in vitro* up to passage 5 showed negligible level of senescence based upon senescence-associated β-galactosidase (SA-β-Gal) activation in about 4% cells (Figure 13).

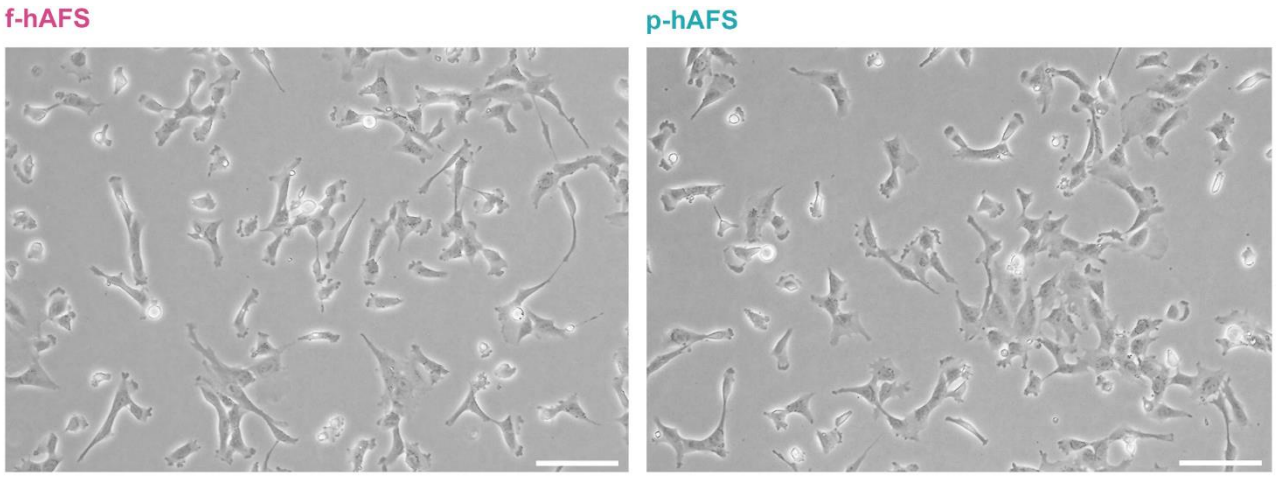

Figure 12 **Fetal and perinatal hAFS morphological evaluation.** Brightfield representative images of fetal hAFS (f-hAFS, left panel) and perinatal hAFS (p-hAFS, right panel) cultured in vitro in standard conditions; scale bar 100 µm.

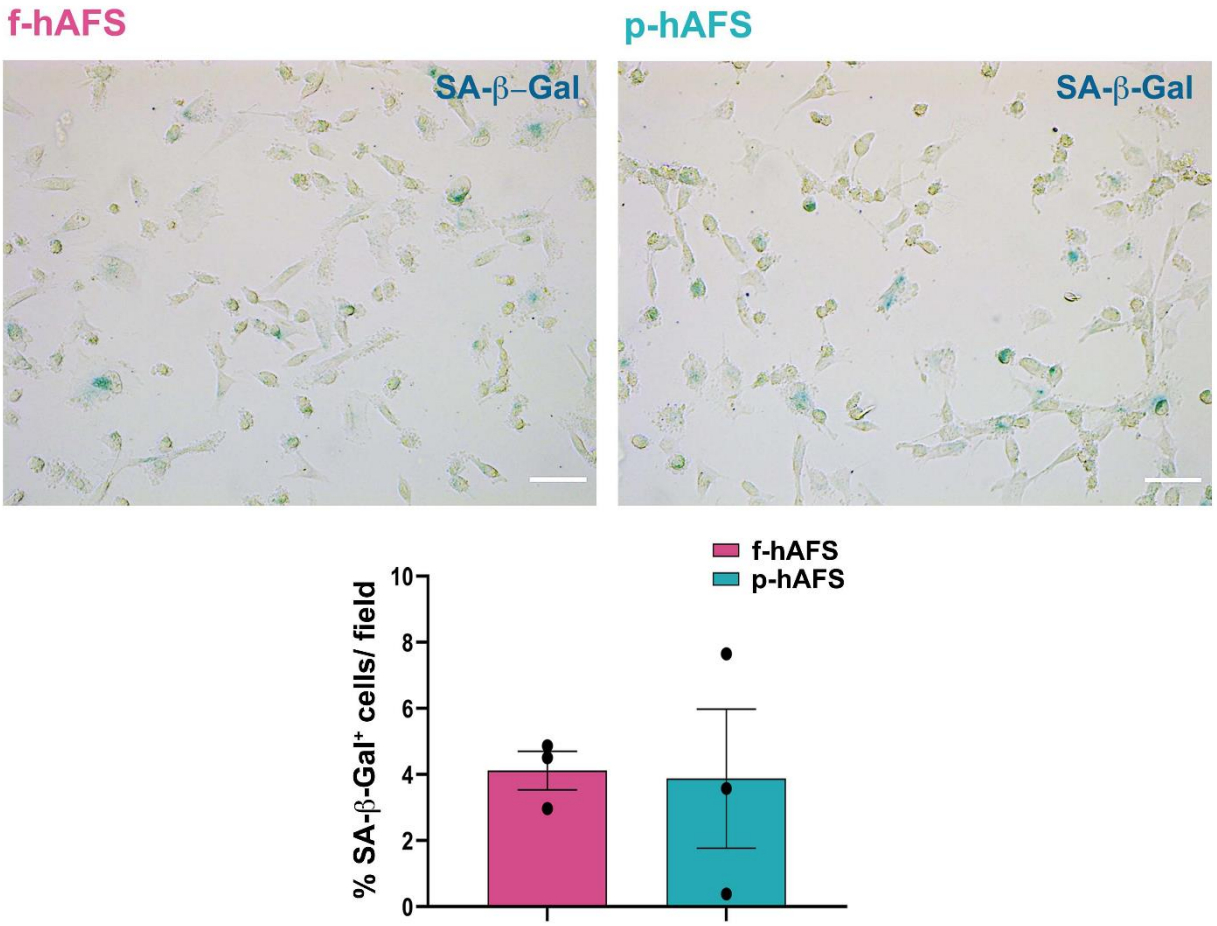

Figure 13 **Fetal and perinatal hAFS senescence evaluation.** Analysis of the senescent marker beta-galactosidase (SA-β-Gal, in blue) via cytochemistry staining on f-hAFS and p-hAFS after 5 passages in culture; representative brightfield images are reported in the upper panel, scale bar 200µm. The corresponding percentage of β-Gal-positive cells/field is reported in the graph in the lower panel (f-hAFS: 4.119±0.5818% and p-hAFS: 3.875± 2.101%; p=0.1424). Data are expressed as mean ± s.e.m of n=3 experiments. Abbreviations: SA-β-gal: Senescence-Associated-β-galactosidase

Furthermore, fetal and perinatal hAFS were phenotypically investigated, specifically for co-expression of CD107a and CD146, which have been recently reported to define a highly secretory phenotype[57]. Cytofluorimetric analysis showed that both f-hAFS and p-hAFS presented high percentage of CD107a+CD146+ cells. In particular, CD107a+CD146+ cells represented the majority of f-hAFS population (*$p<0.05$) being about 63%, while p-hAFS showed a lower enrichment for this subpopulation, by ca. 52% of total cells; nevertheless, this disparity was not statistically significant (Figure 14 B).

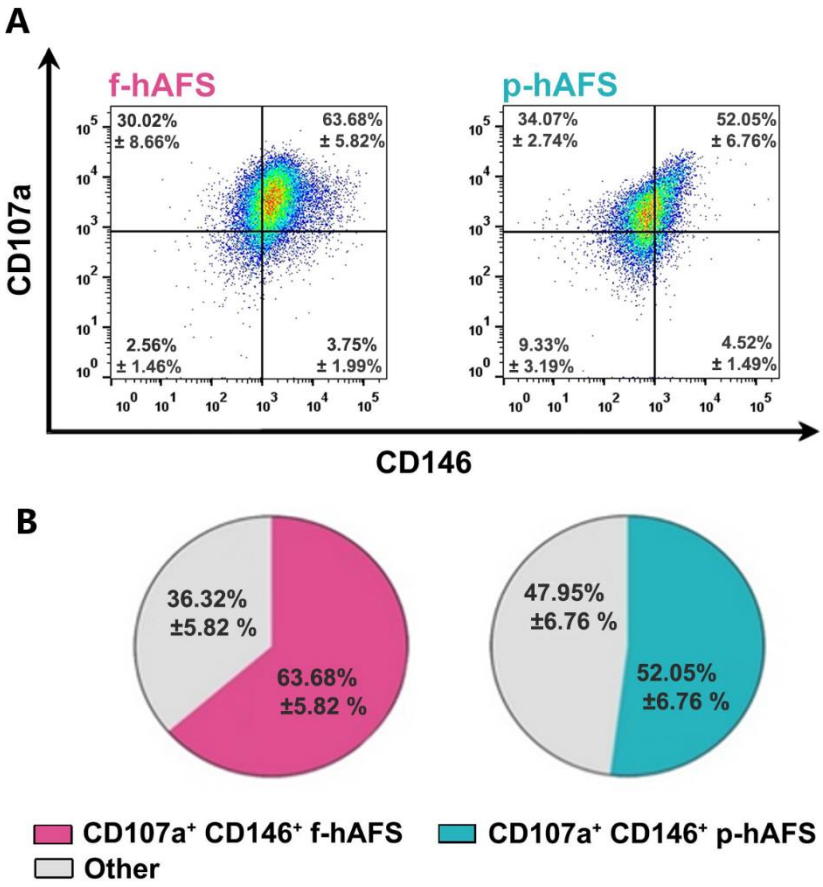

Figure 14 **Immunophenotype of fetal and perinatal hAFS expressing the CD146 and CD107a markers. A.** Representative flow cytometry plots of f-hAFS and p-hAFS and **B**. corresponding values referred to double positive CD107a+CD146+ cells (CD107a+CD146+ f-hAFS: 63.68±5.82%, *p=0.016; CD107a+CD146+ p-hAFS: 52.05%±6.76%, CD107a+CD146+ f-hAFS vs p-hAFS: p=0.2403. Other: total amount of remaining (CD107a-CD146- hAFS, CD107a-CD146+ hAFS and CD107a+CD146- hAFS). Data are expressed as mean ± s.e.m. of n=4 experiments.

4.2 Fetal hAFS show a different metabolism from perinatal hAFS

To assess whether the gestational stage may influence hAFS mitochondrial metabolism, f-hAFS and p-hAFS were analyzed in standard *in vitro* culture conditions by biochemical analyses. The aerobic metabolism was evaluated by OCR and ATP synthesis. The analysis showed that OCR and ATP synthesis were lower in f-hAFS with respect to p-hAFS, when stimulated both with pyruvate + malate (P/M) and with succinate (Figure 15 A-B). Moreover, f-hAFS, but not p-hAFS, displayed lower P/O (oxidative phosphorylation efficiency) values with respect to those reported in the literature[58] (i.e. 2.5 for P/M and 1.5 for succinate) with both substrates, indicating an uncoupling status between OCR and ATP production (Figure 15 C).

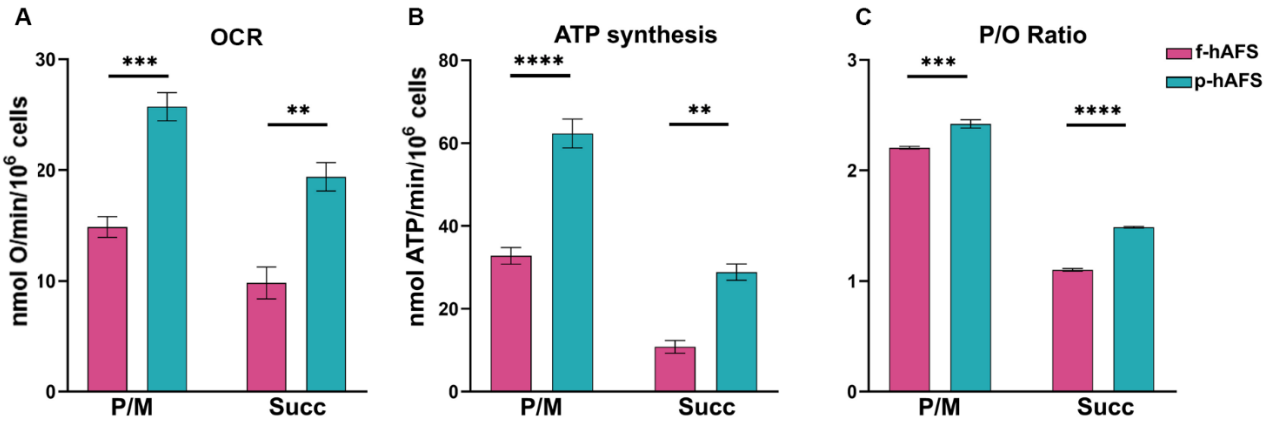

Figure 15 **Mitochondrial oxidative phosphorylation of fetal and perinatal hAFS. A.** The mitochondrial oxygen consumption measured by oximetry as nmol O/min/10^6 cells; **B.** ATP synthesis from the Fo-F1 ATP synthase obtained by luminometry as nmol ATP/min/10^6 cells and **C**. P/O ratio (oxidative phosphorylation efficiency) in f-hAFS and p-hAFS in the presence of pyruvate plus malate (P/M) to stimulate the pathway composed by Complexes I, III, and IV or succinate (Succ) to stimulate the pathway formed by complexes II, III, and IV. **A.** f- hAFS showed a significant reduced oxygen consumption for malate + pyruvate or succinate, respectively, of: 14.87±0.94, 9.820±1.44 nmol O/min/10^6 cells compared to p-hAFS: 25.74±1.27, 19.40±1.28 nmol O/min/10^6 (***$p < 0.001$,$p=0.0005$; **$p < 0.01$,$p=0.0012$). **B.** f-hAFS showed significant reduced ATP synthesis for malate + pyruvate or succinate, respectively, of 32.80±2.03, 10.81±1.55 nmol ATP/min/10^6 cells compared to p-hAFS: 62.33±3.49 and 28.84±1.97 (****$p < 0.0001$; **$p < 0.01$,$p=0.0013$). **C.** f-hAFS P/O ratio values for pyruvate plus malate (P/M) stimulation and succinate, respectively: 2.21±0.01 and 1.10±0.01. p-hAFS P/O ratio values for pyruvate plus malate (P/M) stimulation and succinate, respectively: 2.42±0.04 and 1.49±0.01 (***$p < 0.001$, $p=0.0002$ ****$p < 0.0001$). All data are expressed as mean ± s.e.m and n=3 experiments.

In addition, the relative contributions of glutamine, long-chain fatty acid oxidation, and glucose in the OxPhos (oxidative phosphorylation) metabolism was evaluated through the administration of the respective specific inhibitors: BPTES, Etomoxir, UK5099. It was observed that f-hAFS were sensitive to BPTES and etomoxir, but not to UK5099. By contrast, BPTES and UK5099, but not etomoxir, inhibited the metabolism of p-hAFS. These results indicate that both cell types similarly rely on glutamine as respiratory substrate; yet, f-hAFS preferred fatty acids as a second substrate, while p-hASF were sustained by glucose (Figure 16 A-B).

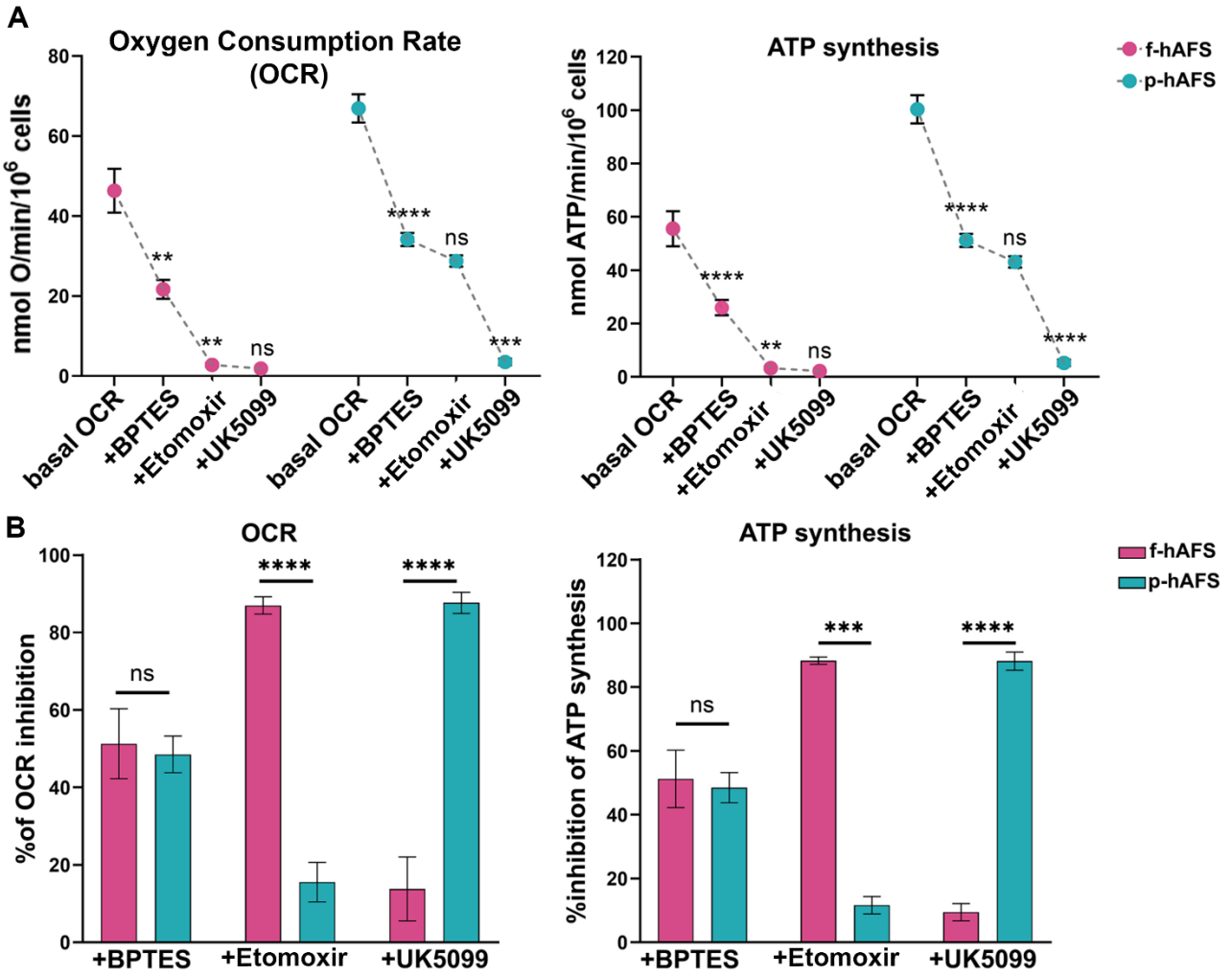

Figure 16 **Energy substrate contribution in oxidative phosphorylation metabolism of f- and p-hAFS. A.** OCR and ATP synthesis in the presence of BPTES, Etomoxir, and UK5099 was evaluated in order to establish the relative contributions of glutamine, long-chain fatty acid oxidation, and glucose to the OxPhos metabolism in f-hAFS and p-hAFS. **B.** The percentage of inhibition of OCR and ATP synthesis due to the molecules indicated above is shown. **A**. f-hAFS showed a significantly reduced oxygen consumption with BPTES and Etomoxir, respectively: 21.67±2.39 nmol O/min/10^6, 2.76±0.41 nmol O/min/10^6, UK5099: 1.87± 0.19 nmol O/min/10^6 **p< 0.01, p=0.0014 and p=0.0088) and a significantly reduced ATP production with the same substrates : 26.00±2.86 nmol ATP/min/10^6, 3.32±0.49 nmol ATP/min/10^6, UK5099: 2.24±0.23 nmol ATP/min/10^6 (****p < 0.0001, **p < 0.01,p=0.0013). p-hAFS showed a significantly reduced oxygen consumption with Etomoxir and UK5099 respectively: 28.75±1.41 nmol O/min/10^6, 3.53±0.79 nmol O/min/10^6 (BPTES: 34.15±1.61 nmol O/min/10^6), (****p < 0.0001). and a reduced ATP production: 43.12±2.11, 5.29±1.18 (BPTES: 51.33±2.41) ****p < 0.0001. **B.** Percentage of OCR inhibition (left panel) in f-hAFS with BPTES, Etomoxir and UK5099, respectively: 51.27%±9.03%, 86.99%±2.2%,13.78%±8.23%, while in p-hAFS it was 48.51%±4.73%, 87.66%±2.73%, and 15.52%±5.11%, respectively (ns: not significant; ****p < 0.0001). Percentage of ATP synthesis inhibition in f-hAFS with BPTES, Etomoxir and UK5099, respectively: 51.27%±9.03%, 88.32%±1.13%, 9.47%±2.71%; and in p-hAFS: 48.51%±4.73%, 11.66%±2.71%, 88.18%±2.84% (****p < 0.0001). All data are expressed as mean ± s.e.m and n=3 experiments.

Finally, the anaerobic metabolism was evaluated by the measurement of glucose consumption and lactate production in hAFS growth medium by spectrophotometric analysis. Interestingly, f-hAFS showed an increment of glucose consumption and lactate release higher than in p-hAFS, resulting in a significantly higher anaerobic glycolysis yield (Figure 17), in order to balance the inefficient aerobic metabolism by lactate fermentation. This difference could also explain the behavior of f-hAFS to the

addition of etomoxir and UK5099. Being glucose principally used through anaerobic glycolysis in f-hAFS, they are likely forced to use fatty acids and glutamine to supply the aerobic metabolism.

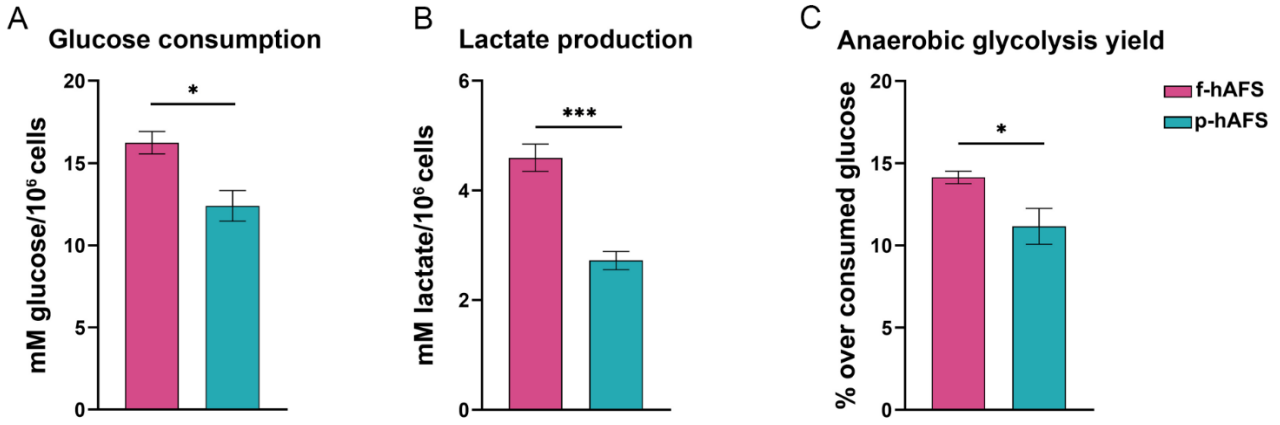

Figure 17 **Anaerobic glycolysis yield in f- and p-hAFS.** Glucose consumption (**A**) and lactate released **(B)** from fetal (pink columns) and perinatal (light blue columns) hAFS, spectrophotometrically measured in the growing medium. **A** Fetal hAFS consume more glucose than perinatal hAFS: 16.23±0.68 and 12.40±0.93 (*p < 0.05,p=0.016) **B** Fetal hAFS produce significantly more lactate respect to perinatal hAFS:4.59±0.25, 2.72±0.16 (***p < 0.001,p=0.0008) **C** Anaerobic glycolysis yield is obtained as the ratio between the lactate produced and the theoretical lactate, calculated as two-fold the consumed glucose. Fetal hAFS hasve an increased anaerobic glycolysis yield in respect to perinatal hAFS: 14.2±0.8 ,11.2±2.2 (*p < 0.05, p=0.0416). All data are expressed as mean ± s.e.m and n=4 experiments.

4.3 Hypoxic preconditioning does not affect fetal and perinatal hAFS viability

In order to analyze the hAFS secretome formulations, cells must be cultured in serum-free conditions, thus avoiding any soluble factor contamination from the fetal bovine serum added to the culture medium. As it has been previously shown, both 24h serum-free (SF) and hypoxic culture conditions (1% O_2) did not significantly alter II trimester f-hAFS viability, while supporting the release of regenerative paracrine factors in the hAFS-conditioned medium (hAFS-CM) and within the extracellular vesicles (hAFS-EVs) that can be isolated from it [3–5,61]. Therefore, in this study it has been assessed whether p-hAFS showed a similar behavior under the same SF and hypoxic preconditioning regime. To this end, f-hAFS and p-hAFS viability was analyzed through cytofluorimetry, utilizing an Annexin V and PI expression assay, after 24h *in vitro* culture under the following settings: normoxic condition (20% O_2) in complete control (Ctrl) culture medium (Ctrl f-$hAFS_{normo}$ and Ctrl p-$hAFS_{normo}$), normoxic condition in SF medium (SF f-$hAFS_{normo}$ and SF p-$hAFS_{normo}$), hypoxic condition (1% O_2) in complete control medium (Ctrl f-$hAFS_{hypo}$ and Ctrl p-$hAFS_{hypo}$), and hypoxic condition in SF medium (SF f-$hAFS_{hypo}$ and SF p-$hAFS_{hypo}$).

f-hAFS viability was confirmed to remain unaltered in both Ctrl and SF conditions and, under hypoxic stimulation, with more than 80% (up to almost 88%) of total cells being unaffected, with early and

late apoptotic cells ranging from ca. 13% to 18% in SF conditions, without any statistically significant relevance. Likewise, perinatal hAFS viability was in the range of 82-92%, with early and late apoptotic cells being up to 18% in SF conditions. However, p-hAFS were marginally disturbed only under the combined hypoxic and SF conditions. Indeed, hypoxic preconditioning did not influence cell survival when p-hAFS were cultured in complete medium, while the corresponding SF condition showed a statistically significant (*$p<0.05$) increase by ca. 4-fold in the amount of late apoptotic cells (Figure 18 A-B and Table 1).

Table 1 Percentage values of apoptosis analysis on f- and p- hAFS in different conditions.

		$Ctrl_{normo}$	SF_{normo}	$Ctrl_{hypo}$	SF_{hypo}
f- hAFS	Live	87.70 ±3.86%	86.70 ± 5.21%	87.02 ± 4.38%	81.20 ± 6.53%
	Early apoptotic	9.83 ±3.75%	8.80 ± 3.54%	8.72 ± 3.61%	12.90 ± 5.07%
	Late Apoptotic	2.20 ± 0.41%	3.90 ± 1.68%	3.22 ± 1.08%	5.11 ± 2.22%
p-hAFS	Live	89.40 ±1.92%	82.20 ± 3.64%	92.44 ± 1.63%	80.01 ±4.76%
	Early apoptotic	6.54 ± 2.22%	7.40 ±1.73%	4.15 ± 1.35%	6.40 ±1.83%
	Late Apoptotic	3.70± 0.87%	9.34 ± 2.25%	2.90 ± 1.12%	12.31 ±3.82%

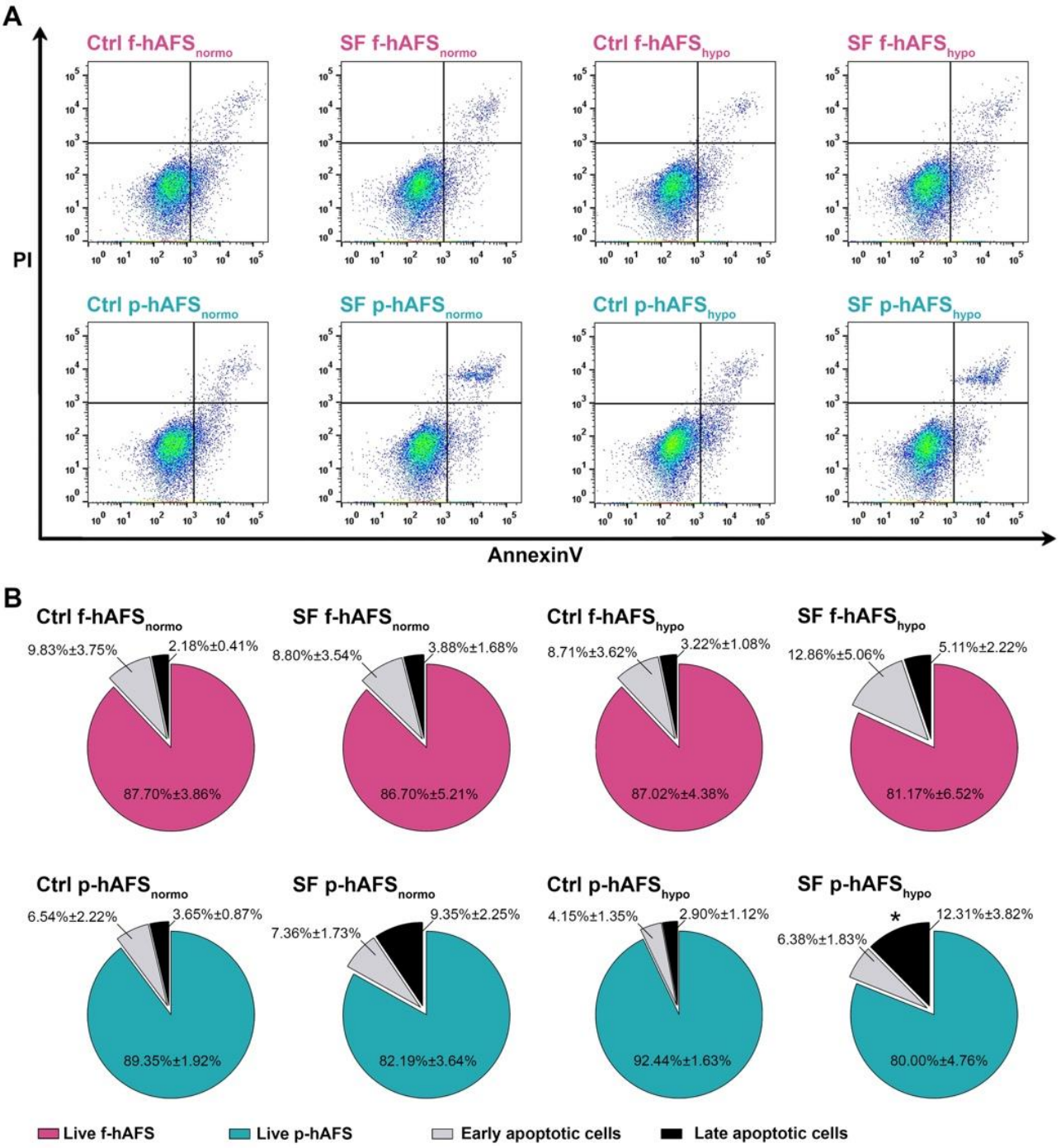

Figure 18 **Evaluation of the preconditioning effect on fetal and perinatal hAFS viability. A.** Representative graphs of apoptosis analysis by flow cytometry evaluation of PI and Annexin V expression on f-hAFS and p-hAFS experiencing 24h preconditioning in either 20% O_2 normoxic condition as compared to 1% O_2 hypoxic one and in complete control (Ctrl) medium versus serum-free (SF) medium (Ctrl f-hAFS$_{normo}$; Ctrl f-hAFS$_{hypo}$; SF f-hAFS$_{normo}$; SF f-hAFS$_{hypo}$; Ctrl p-hAFS$_{normo}$; Ctrl p-hAFS$_{hypo}$; SF p-hAFS$_{normo}$; SF p-hAFS$_{hypo}$, respectively). **B.** Upper panel: pie charts of live (pink), early apoptotic (gray) and late apoptotic (black); lower panel pie charts of live (blue), early apoptotic (gray) and late apoptotic (black) p-hAFS. *late apoptotic Ctrl p-hAFS$_{hypo}$ vs SF p-hAFS$_{hypo}$*: *p = 0.0392; no statistically significant differences were detected among all other comparisons. Values are expressed as mean ± s.e.m of at least n=4 independent experiments in Table 1.

4.4 Hypoxic preconditioning sustains both fetal and perinatal hAFS secretory activity

Next, the yield of secretome fractions obtained from f-hAFS versus p-hAFS was evaluated, based on their protein enrichment. The total hAFS secretome, as the whole of cell-secreted paracrine factors, is here represented by the hAFS-CM. The protein concentration of f-hAFS-CM and p-hAFS-CM following hypoxic vs normoxic preconditioning in SF medium (namely, f-hAFS-CM_{normo}, f-hAFS-CM_{hypo}, p-hAFS-CM_{normo}, and p-hAFS-$CM_{hypo,}$) was evaluated by BCA assay and measured per secreting 10^6 cells. The results acquired suggested that f-hAFS-CM and p-hAFS-CM showed an equal positive trend in protein enrichment following hypoxic preconditioning (f-hAFS-CM_{hypo}: 166.10±22.13µg/10^6 cells and p-hAFS-CM_{hypo}: 182.30±29.71µg/10^6 cells) in respect to their normoxic counterparts (f-hAFS-CM_{normo}: 105.50±19.89µg/10^6 cells and p-hAFS-CM_{hypo}: 91.12± 24.39µg/10^6 cells). Likewise, the protein concentration of hAFS-EVs separated by ultracentrifugation from the corresponding hAFS-CM was measured in the following groups: f-hAFS-EVs_{normo}, f-hAFS-EVs_{hypo}, p-hAFS-EVs_{normo}, and p-hAFS-$EVs_{hypo.}$ EVs showed a comparable yield of their surface protein amount when obtained from f-hAFS or p-hAFS. As for hAFS-CM formulations, a positive trend in the increase of protein content on f-hAFS-EV and p-hAFS-EV was appreciated after hypoxic stimulation in respect to the corresponding normoxic condition (f-hAFS-EVs_{hypo}: 2.03±0.67µg/10^6 cells and p-hAFS-EVs_{hypo}: 1.85±0.47µg/10^6 cells; f-hAFS-EVs_{normo}: 1.28±0.36µg/10^6 cells and p-hAFS-EVs_{normo}: 1.19±0.31µg/10^6 cells, Figure 19).

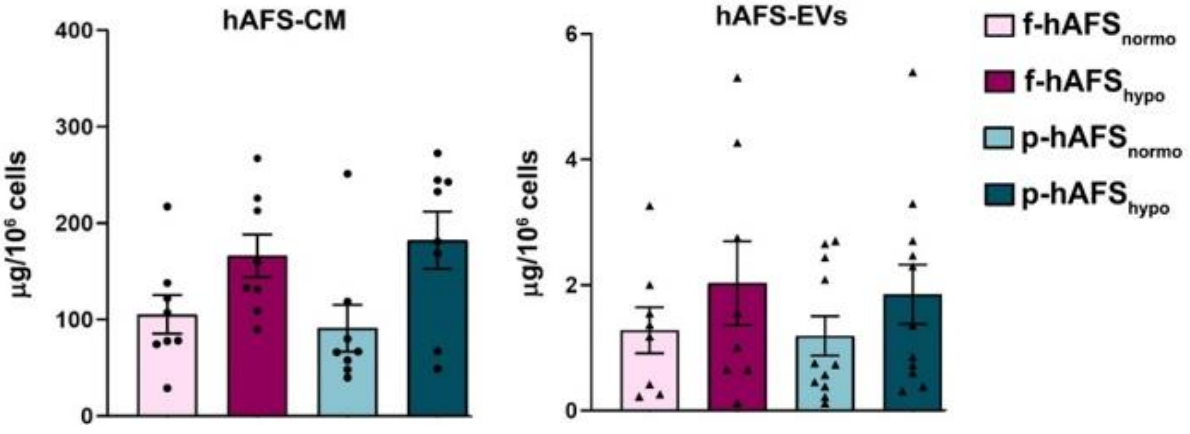

Figure 19 **Evaluation of fetal and perinatal hAFS secretome fraction yield**. hAFS secretome fraction yield was evaluated by BCA assay for protein concentration under serum-free conditions. Left panel refers to the protein content of the whole secretome, namely the in vitro hAFS-conditioned medium (hAFS-CM), as following: f-hAFS-CM_{normo} (105.50±19.89µg/10^6cells); f-hAFS-CM_{hypo} (166.10±22.13 µg/10^6cells); p-hAFS-CM_{normo} (91.12 ± 24.39 µg/10^6cells) and p-hAFS-CM_{hypo} (182.30±29.71 µg/10^6cells), n=6 experiments. Right panel refers to hAFS-EV protein content (hAFS-EVs), as following: f-hAFS-EVs_{normo} 1.28±0.36 µg/10^6cells); f-hAFS-EVs_{hypo} (2.03±0.67 µg/10^6cells), n=8 experiments, and p-hAFS-EVs_{normo} (1.19±0.31 µg/10^6cells) and p-hAFS-EVs_{hypo} (1.85±0.47 µg/10^6cells), n=11 experiments. Values are expressed as mean ± s.e.m of independent experiments.

4.5 Fetal and perinatal hAFS release EVs with analogous morphology and size distribution

Morphological analysis by TEM highlighted the high secretory prolife of both f-hAFS and p-hAFS releasing EVs (Figure 20 A). Furthemore, the size, area, and mean gray value of f-hAFS-EVs vs. p-hAFS-EVs (Figure 20 B) following hypoxic preconditioning was investigated. Fetal and perinatal hAFS released EVs heterogeneous in size, in the range of 40-250 nm, hence including both exosomes/small EVs and microvesicles/shedding vesicles. The average size of EVs/field in the different groups was comparable, with fetal hAFS-EVs measuring around 90-100 nm (f-hAFS-EVs_{normo}: 104.00±3.00nm; f-hAFS-EVs_{hypo}: 97.10±10.10nm) and perinatal ones being about 70-114 nm (p-hAFS-EVs_{normo}: 94.60±19.53nm; p-hAFS-EVs_{hypo}: 76.43±4.86nm). As for the yield, hAFS stimulated under hypoxia showed a positive trend in the increase of the amount of small EVs, although no statistically significant differences were observed. f-hAFS-EVs_{hypo} measuring between 40-70nm almost doubled as compared to their normoxic counterpart and p-hAFS-EVs_{hypo} between 40-70 nm, 70-100 nm and 100-130 nm were almost triple in the amount in respect to the normoxic ones (Figure 20 B and Table 2).

Table 2 f-hAFS-EVs and p-hAFS-EVs number per field by TEM analysis

Size distribution	f-hAFS-EVs $_{normo}$	f-hAFS EVs $_{hypo}$	p-hAFS EVs $_{normo}$	P hAFS-EVs $_{hypo}$
220-250nm	4.00±1.16	4.33±0.33	1.33±0.67	0.67±0.67
190-220nm	8.33±1.86	6.00±1.15	3.00±0.57	2.67±1.20
160-190nm	13.00±0.57	13.66±2.03	4.33±1.76	5.33±1.66
130-160nm	33.00±9.61	39.00±3.21	11.00±6.36	19.33±11.84
100-130nm	51.67±13.30	55.66±6.64	15.33±6.36	56.00±32.56
70-100nm	58.66±10.49	88.66±38.52	28.00±10.21	73.00±48.50

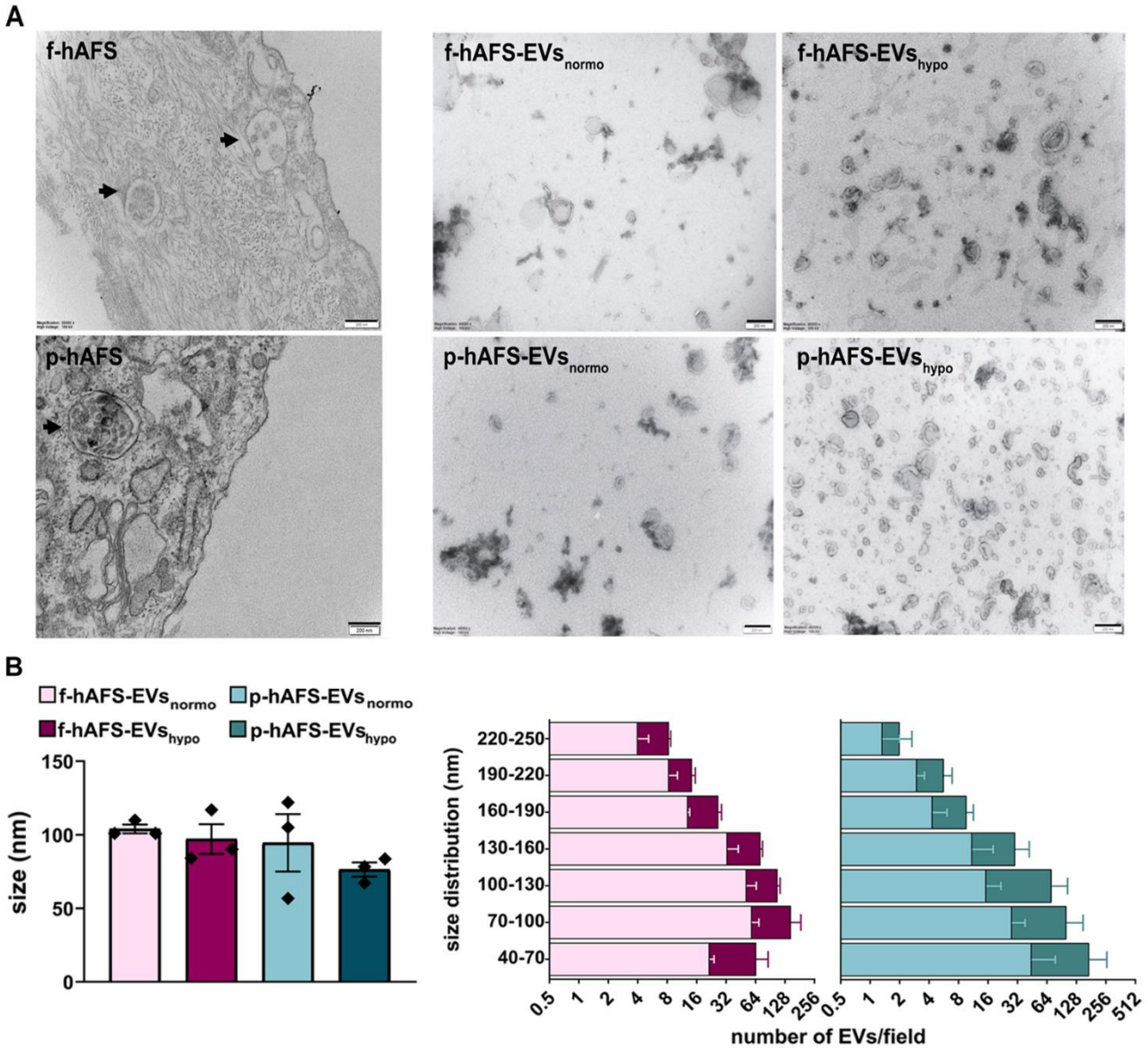

Figure 20 **Morphological characterization of fetal and perinatal hAFS-EVs by transmission electron microscopy. A.** Representative images of transmission electron microscopy (TEM) of: f-hAFS and p-hAFS (upper and lower left panels, respectively; black arrows indicate intracytoplasmic multi-vesicular bodies with small EVs/exosomes within them) and of f-hAFS-EVs and p-hAFS-EVs (upper and lower right panels, respectively) separated from the conditioned medium released by corresponding hAFS in serum-free conditions and under normoxic versus hypoxic preconditioning (f-hAFS-EVs$_{normo}$; f-hAFS-EVs$_{hypo}$; p-hAFS-EVs$_{normo}$; and p-hAFS-EVs$_{hypo}$, respectively), scale bars: 200nm. **B.** Left panel: hAFS-EVs size distribution among different conditions by TEM analysis: f-hAFS-EVs$_{normo}$: 104.00±3.00nm; f-hAFS-EVs$_{hypo}$: 97.10±10.10nm; p-hAFS-EVs$_{normo}$: 94.60±19.53nm; p-hAFS-EVs$_{hypo}$: 76.43±4.86nm. Right panel: values are reported in Table 2. Values are expressed as mean ± s.e.m of n=3 independent experiments.

Moreover, nanoparticle tracking analysis (NTA) showed an elevated number of particles in both f-hAFS-EVs and p-hAFS-EVs preparations, confirming an equivalent positive trend of increase in the hypoxic samples as for previous analyses (f-hAFS-EVs$_{normo}$: 1.82±0.12×10^9 particles/10^6 cells; f-hAFS-EVs$_{hypo}$: 3.29±0.27x10^9 particles/10^6 cells; p-hAFS-EVs$_{normo}$: 2.43±0.81x10^9 particles/10^6 cells; p-hAFS-EVs$_{hypo}$: 3.05±0.62x10^9 particles/10^6 cells, Figure 21 A-B).

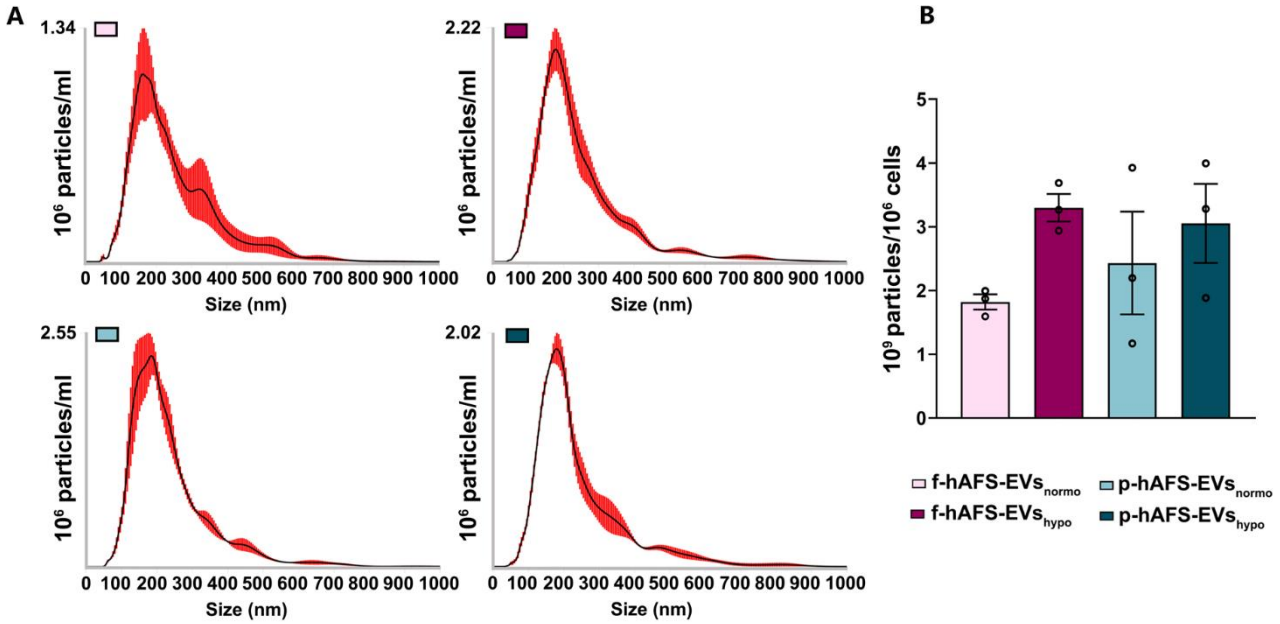

Figure 21 **Nanoparticle tracking analysis for hAFS-EV size and distribution**. **A**. Representative image of the graphical output. **B.** hAFS-EVs concentration measured as 10^9 particles per 10^6 secreting cells: f-hAFS-EVs$_{normo}$: 1.82±0.12x10^9 particles/10^{6}cells; f-hAFS-EVs$_{hypo}$ 3.29±0.27x10^9 particles/10^{6}cells; p-hAFS-EVs$_{normo}$: 2.43±0.81x10^9 particles/10^{6}cells, and p-hAFS-EVs$_{hypo}$: 3.05±0.62x10^9 particles/10^{6}cells; values are expressed as mean ± s.e.m of n=3 independent experiments

4.6 Proteomic characterization of fetal- and perinatal hAFS secretome fractions shows different profiles

In order to complete the characterization of both f-hAFS and p-hAFS secretome composition from a proteomic point of view, the analysis of their protein content was performed by mass spectrometry. Results were analyzed and evaluated in collaboration and with the help of Dr. Antonella De Palma e Dr. Rossana Rossi from the Proteomics and Metabolomics Unit, Institute for Biomedical Technologies (ITB-CNR), Milan.

A total of 4179 distinct proteins were identified with at least one unique peptide, molecular weights ranging from 2 to 3900 kDa and isoelectric points from 3.6 to 13, showing an average protein expression higher in hAFS-EVs compared to hAFS-CM. To quantitatively examine the proteomic

changes, a label-free differential analysis was performed, using the home-made MAProMa software and applying its two algorithms, DAve and DCI, representing the ratio and the confidence in differential expression, respectively, on the aPSMs of each single protein between the two compared terms. Using stringent filters for DAve and DCI to maximize the identification confidence and to consider proteins with a variation greater than a fold change of 1.5, the pairwise comparisons of f-hAFS-EVs versus p-hAFS-EVs and f-hAFS-CM versus p-hAFS-CM were carried out. Gene Ontology (GO) enrichment analysis with FunRich tool was performed in order to compare the abundance of GO terms in the dataset against their natural abundance in the reference dataset and to find statistically over-represented groups of proteins, according to their molecular functions and involvement in biological process.

Regarding molecular functions, hAFS-CM was enriched with constituents of extracellular matrix and cytoskeleton, cytoskeletal protein binding and structural molecule activity, while hAFS-EVs were enriched in structural constituents of cytoskeleton and ribosome, DNA and RNA binding and GTPase and chaperone binding factors (Figures 22-23). Regarding biological processes, the majority of proteins contained in both h-AFS-EVs and h-AFS-CM belonged to cell growth/maintenance and protein metabolism (Figures 24-25).

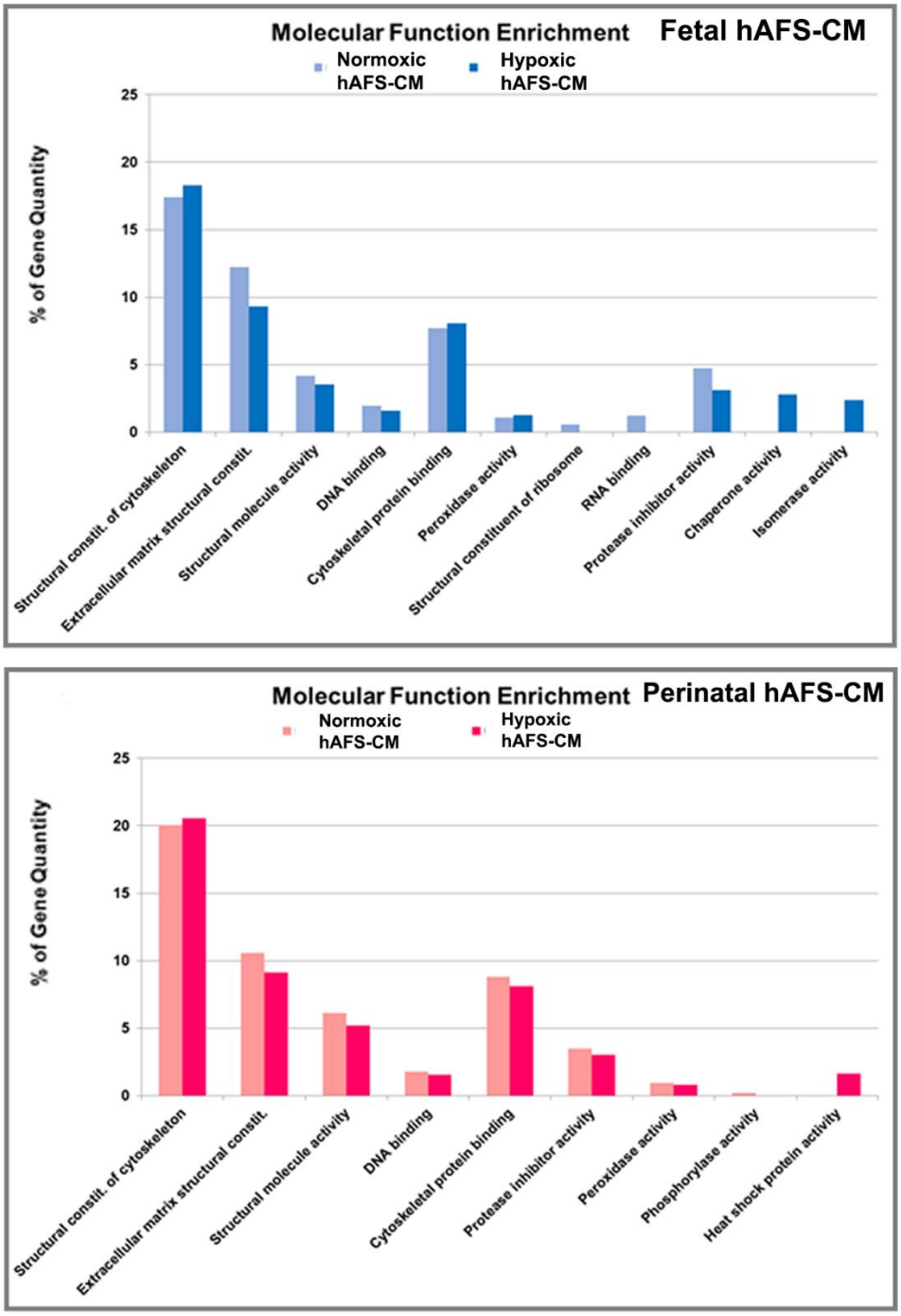

Figure 22 Molecular function enrichment of fetal and perinatal hAFS-CM

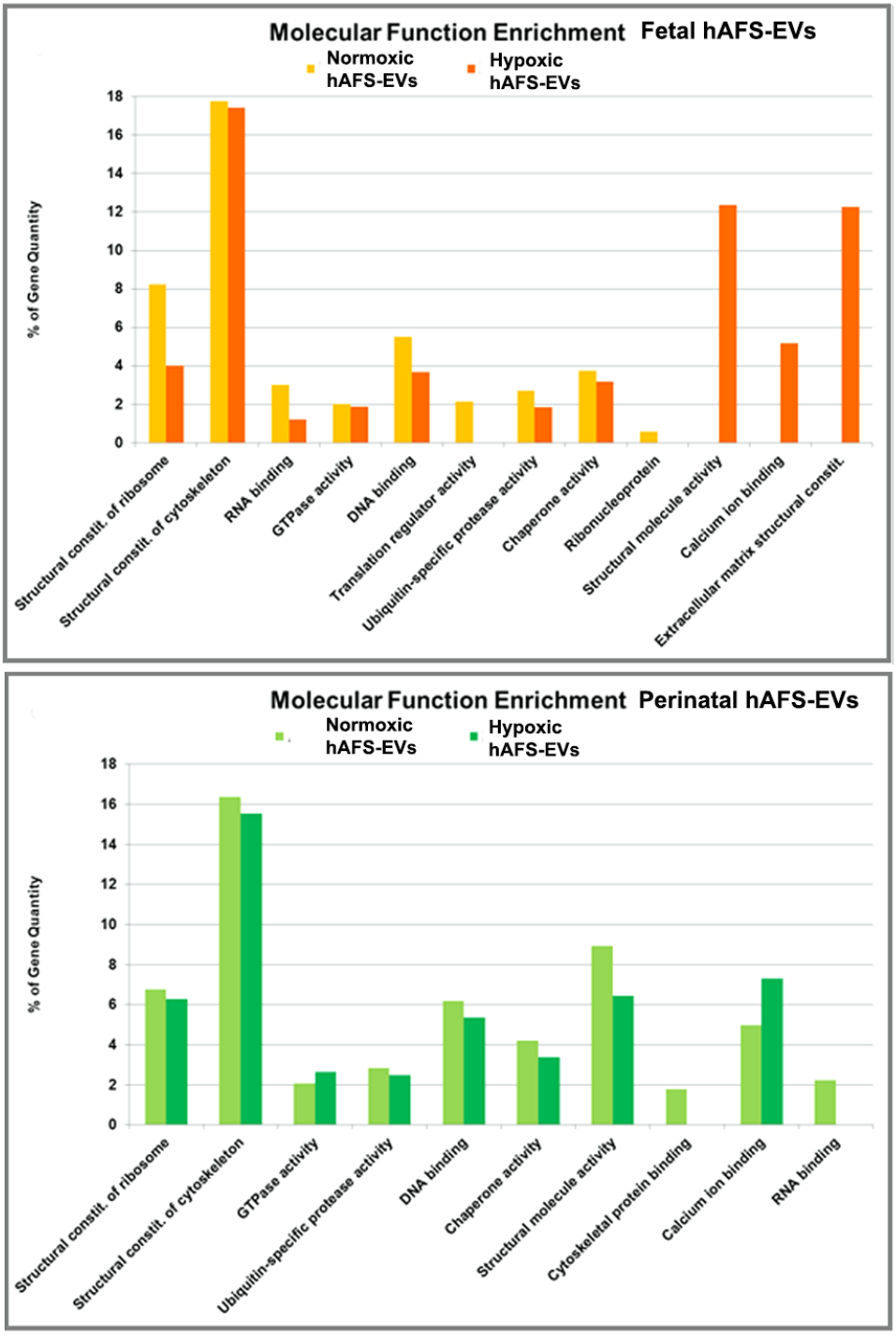

Figure 23 Molecular function enrichment in hAFS-EVs from proteomic analysis

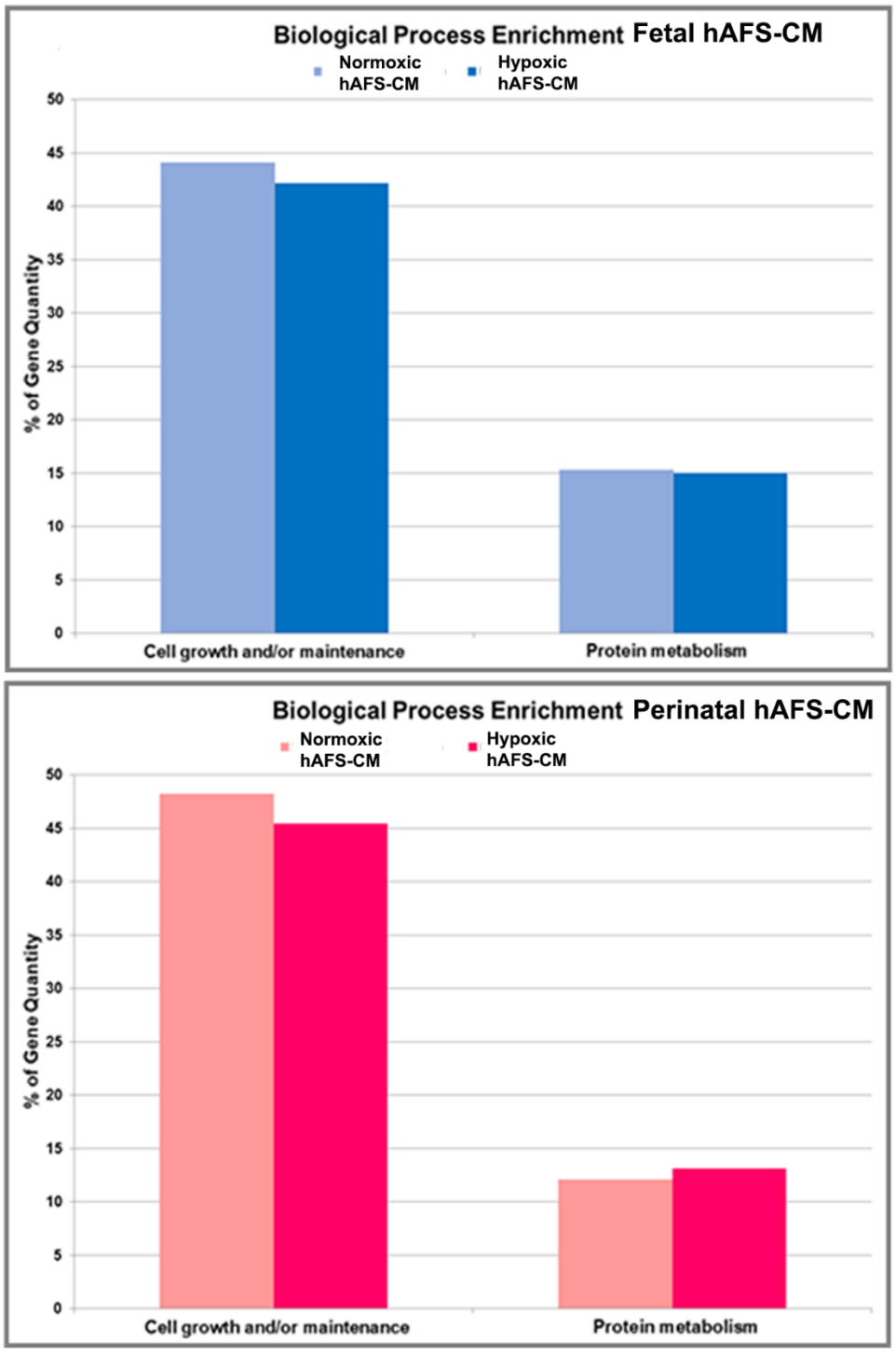

Figure 24 Biological processes enrichment in hAFS-CM from proteomic analysis

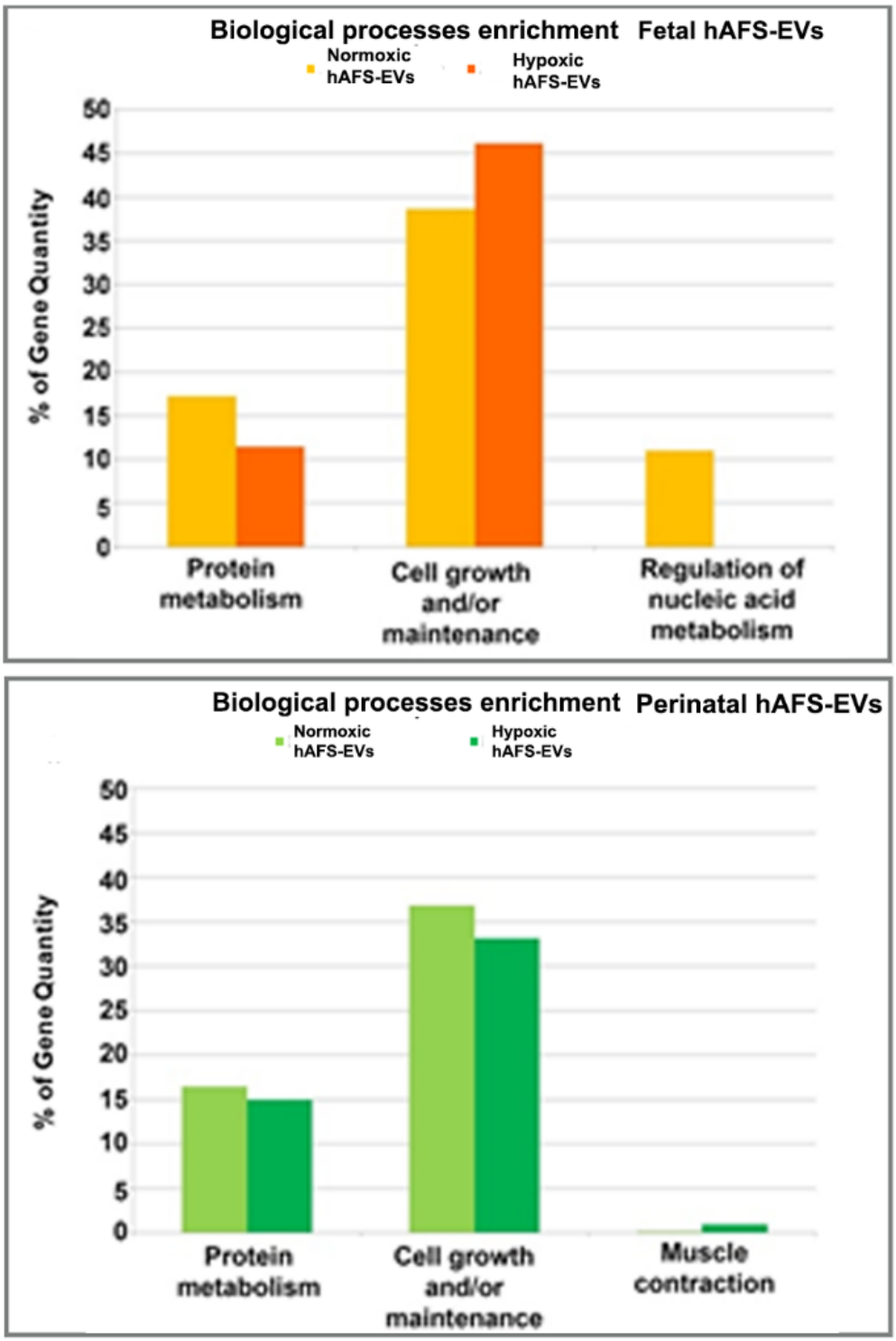

Figure 25 Biological processes enrichment in hAFS-EVs from proteomic analysis

The most interesting data concern hAFS-EVs, in which the difference between gestational ages appeared to be mostly dependent on hypoxic preconditioning, resulting in the enrichment of "extracellular matrix structural constituents", including the proteoglycan Agrin (O00468) and one of its potential isoform (A0A494C0G5) (Figures 26A-B).

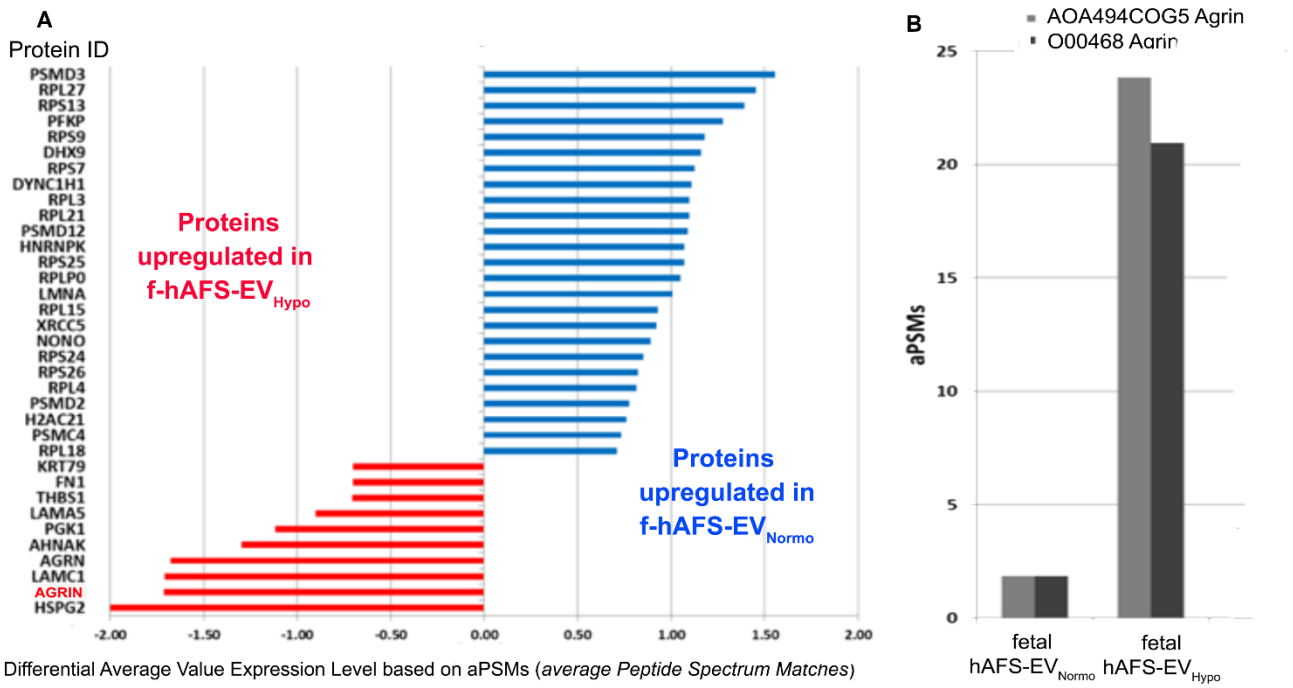

Figure 26 **A.** Proteomic analysis for the differential expression of proteins within the hAFS-EVs obtained by hAFS cells cultured in normoxic (red) versus hypoxic conditions (blue) with p<0.0001 (f-hAFS-EVNormo and -EVs f-hAFS-EVHypo, respectively; agrin is highlighted in red). **B.** Level of the expression of Agrin main isoform and of its potential isoform (O00468 and A0A494C0G5) f-hAFS-EV$_{Normo}$ versus f-hAFS-EV$_{Hypo}$. aPSMs: average Peptide Spectrum Matches.

4.7 The cytokine and chemokine profiling of fetal vs perinatal hAFS-CM and hAFS-EVs revealed different distribution patterns

The regenerative influence of f-hAFS-CM$_{hypo}$ on injured cardiovascular cells via paracrine effects has been previously validated [4,5,61]. Here, the cytokine and chemokine content of f-hAFS-CM$_{hypo}$ versus the corresponding perinatal hAFS counterpart has been investigated (Figure 27 and Table 3); this analysis revealed that some cytokines/chemokines were differentially expressed between the two groups.

Angiogenin, Extracellular Matrix Metalloproteinase Inducer (EMMPRIN), Interleukin 8 (IL-8), and Monocyte Chemoattractant Protein-1 (MCP-1) were found to be exclusively enriched in the f-hAFS-CM$_{hypo}$, and not detected at all in the p-hAFS-CM$_{hypo}$. Insulin-like growth factor binding protein 2

(IGFBP2) and Osteopontin (OPN) were significantly increased in f-hAFS-CM_{hypo} in respect to p-hAFS-CM_{hypo} by 3.5- and 3.8-fold (*$p<0.05$ and **$p<0.01$, respectively, Figure 5A). Other cytokines were detectable at low levels, namely Cystatin C (CST3), Fibroblast Growth Factor 19 (FGF19), Interleukin-17a (IL-17a), Macrophage Migration Inhibitor Factor (MIF), Pentraxin 3 (PTX3); Plasminogen Activator Inhibitor-1 (PAI-1) was detected by a strong signal and found correspondingly expressed in both f-hAFS-CM_{hypo} and p-hAFS-CM_{hypo} (Figure 27).

While fetal- versus perinatal hAFS-CM showed differential expression in their cytokine and chemokine profile, the corresponding fetal versus perinatal EV counterparts were more homogeneously distributed, although with lower expression (Figure 28 and Table 4). Nonetheless, some differences could be appreciated: Dipeptidyl-Peptidase IV (DPPIV), Growth/differentiation factor 15 (GDF-15) and Interleukin 18 (IL-8) were expressed only by f-hAFS-EVs_{hypo}, although at quite low level; Angiopoietin 2, CD40 Ligand, and Vitamin D-Binding Protein (VDBP) were found only in p-hAFS-EVs_{hypo}, despite being detected in low amounts. Other measurable cytokines such as Brain-derived Neurotrophic Factor (BDNF), Endoglin, FGF-19, Insulin-like growth factor binding protein 3 (IGFBP3), IL-17a, MIF, OPN, PTX3, and Stromal Derived Factor-1 alpha (SFD-1α), were found in both f-hAFS-EVs_{hypo} and p-hAFS-EVs_{hypo}, with PAI-1 and EMMPRIN giving a stronger signal (Figure 28).

BDNF, Endoglin, IGFBP3, and SDF-1a were exclusively enriched in hypoxic hAFS-EVs compared to the corresponding hAFS-CM, regardless of gestational stage. Moreover, while EMMPRIN was not detected within the p-hAFS-CM_{hypo}, it was found enriched in the EV corresponding fraction; conversely, OPN was more abundant in f-hAFS-CM_{hypo} than in f-hAFS-EVs_{hypo}, while being comparable in the corresponding perinatal hAFS secretome fractions. FGF-19, MIF, and PTX3 were similarly expressed in both fetal- and perinatal hAFS-CM and the corresponding hAFS-EVs, with PAI-1, being highly enriched in all hypoxic secretome fractions.

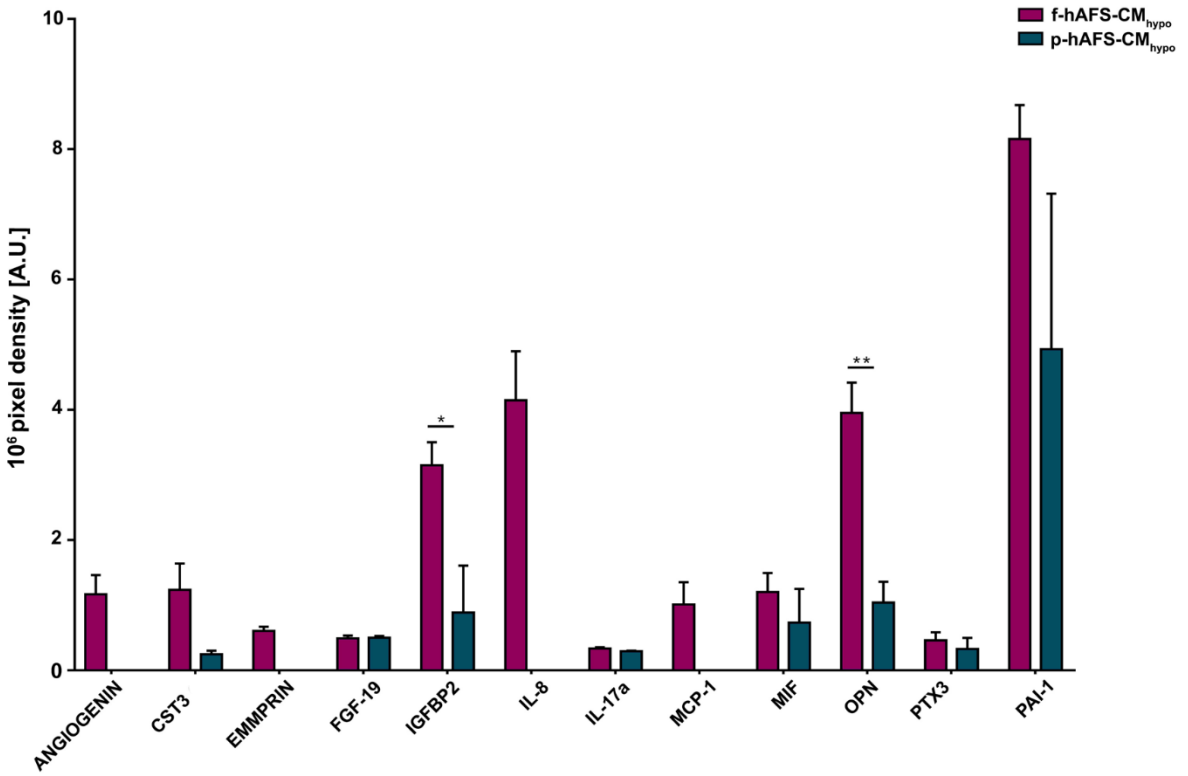

Figure 27 **Cytokine and chemokine evaluation in fetal and perinatal hAFS-CM. A.** Expression of cytokines and chemokines detected within fetal- versus perinatal hypoxic hAFS-CM (f-hAFS-CM_{hypo} vs p-hAFS-CM_{hypo}) by array analysis are reported in pixel density by arbitrary units [A.U.]**;** *p = 0.0485; **p = 0.0067. Values are expressed as mean ± s.e.m of n=3 independent experiments and are reported in Table 3.

Table 3

	f-hAFS-CM_{hypo}	**p-hAFS-CM_{hypo}**
ANGIOGENIN	1.16636953 ± 0.29883221	n.d.
CST3	1.23531432 ± 0.40724366	0.24749743 ± 0.05417413
EMMPRIN	0.60693284 ± 0.06384752	n.d.
FGF-19	0.48995348 ± 0.4774637	0.50153070 ± 0.02696120
IGFBP-2	3.1474948 ± 0.35619519	0.88468344 ± 0.72349074
IL-8	4.14571707 ± 0.75267900	n.d.
IL-17a	0.33512130 ± 0.02035.60	0.29081466 ± 0.01026642
MCP-1	1.01004149 ± 0.34537853	n.d.
MIF	1.20132892 ± 0.29595724	0.73015821 ± 0.52329208
OPN	3.95352711 ± 0.46281117	1.04109906 ± 0.32145075
PTX3	0.46048569 ± 0.12506492	0.32781099 ± 0.17373157
PAI-1	8.15728670 ± 0.52230005	4.929970058 ± 2.38753363

Quantification of detectable chemokines/cytokines within f- and p-hAFS-CM fractions obtained following hypoxic preconditioning of secreting cells. Values refer to pixel intensity and are expressed as arbitrary units ± s.e.m.; the undetectable spots of chemokines are classified not determined (n.d.). CST3: Cystatin C; EMMPRIN: Extracellular Matrix Metalloproteinase Inducer; FGF19: Fibroblast Growth Factor 19; IGFBP2: Insulin-like growth factor binding protein 2; IL-8: Interleukin 8; IL-17a: Interleukin 17a; OPN: Osteopontin; PTX3: Pentraxin 3; PAI-1: Plasminogen Activator Inhibitor-1.

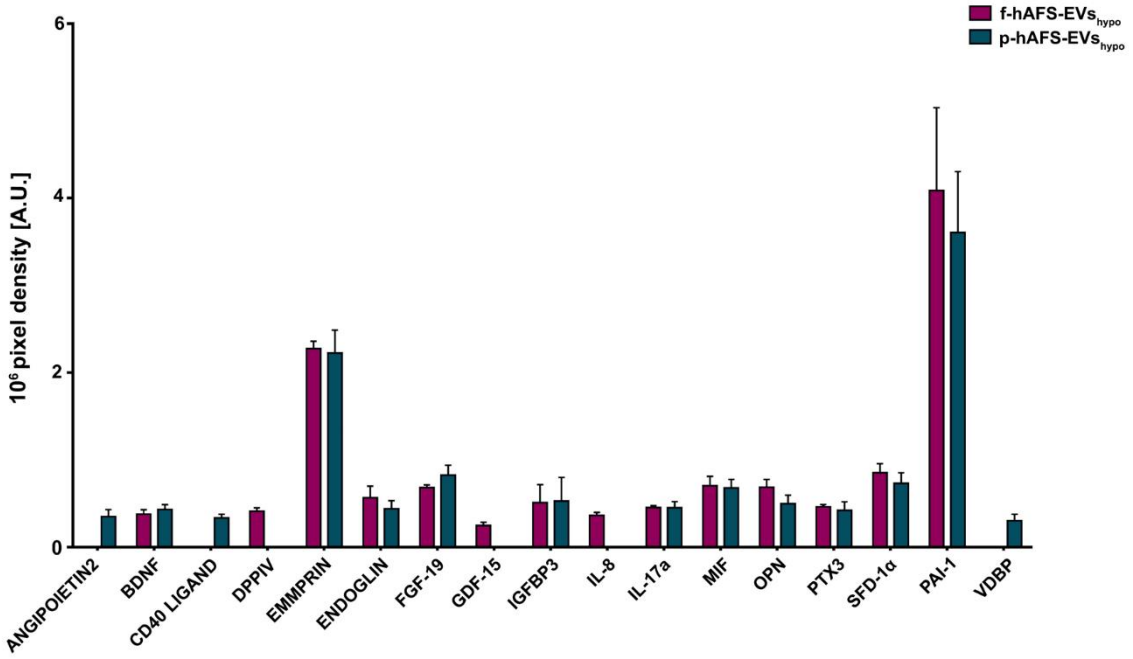

Figure 28 **Cytokine and chemokine evaluation in fetal and perinatal hAFS-EVs.** Cytokine and chemokine content detected in fetal- versus perinatal hypoxic hAFS-EVs (f-hAFS-EVs$_{hypo}$ vs p-hAFS-EVs$_{hypo}$) by array analysis and expressed by pixel density as arbitrary units [A.U.]. Values are expressed as mean ± s.e.m of n=3 independent experiments and are reported in Table 4.

Table 4

	f-hAFS-EVs$_{hypo}$	**p-hAFS-EVs$_{hypo}$**
ANGIOPOIETIN2	2.2862903 ± 0.7832655	3.5070887 ± 0.8142010
BDNF	3.8037476 ± 0.05111936	4.3545673 ± 0.05496117
CD40L	n.d.	3.375377 ± 0.4268069
DPPIV	4.117405 ± 0.04090764	n.d.
EMMPRIN	22.74630 ± 0.8738339	22.2322633 ± 2.67528.58
ENDOGLIN	5.6782133 ± 1.3366492	4.405629 ± 0.9575114
FGF-19	6.854674 ± 0.3063227	8.259132 ± 1.1532451
GDF-15	2.4901123 ± 0.3842588	n.d
IGFBP-3	5.1119277 ± 2.0812600	5.2924323 ± 2.7215211
IL-8	3.6591423 ± 0.3329946	n.d.
IL-17a	4.561738 ± 0.2201049	4.5416947 ± 0.6909609
MIF	7.057947 ± 1.0714464	6.8113843 ± 0.98072733
OPN	6.893473 ± 0.9002976	4.9828363 ± 1.0135084
PTX3	3.46375177 ± 0.2707602	4.220527 ± 0.9966829
SDF-1α	8.5380787 ± 1.0474851	7.314309 ± 1.2246857
PAI-1	40.8777033 ± 9.4905114	36.05712 ± 7.0041352
VDBP	n.d.	3.042418 ± 0.7605829

Quantification of detectable chemokines/cytokines within f- and p- hAFS-EV fractions obtained following hypoxic preconditioning of secreting cells. Values refer to pixel intensity and are expressed as arbitrary units mean ± s.e.m.; the undetectable spots of chemokines are classified not determined (n.d.). BDNF: Brain-derived neurotrophic factor; CD40L: CD40 LIGAND; DPPIV: Dipeptidyl-peptidase IV; EMMPRIN: Extracellular Matrix Metalloproteinase Inducer; FGF19: Fibroblast Growth Factor 19; GDF-15: Growth/differentiation factor 15; IGFBP-3: IGFBP3: Insulin-like growth factor binding protein 3; IL-8; Interleukin 8; IL-17a: Interleukin 17a; OPN: Osteopontin; PTX3: Pentraxin 3; SFD-1 α: Stromal Derived Factor-1alpha; PAI-1: Plasminogen Activator Inhibitor-1; VDBP: Vitamin D binding protein.

4.8 In vitro proliferative paracrine effects of hypoxic fetal vs perinatal hAFS-CM and hAFS-EVs on mNVCM

Since previous results showed that hypoxic fetal hAFS secretome (both soluble fraction and EVs) induced stimulatory effects *in vivo*, in a preclinical mouse model of myocardial infarction[5], in this study the cardio-proliferative potential of hypoxic fetal versus perinatal hAFS-CM and hAFS-EVs was evaluated *in vitro*. Neonatal cardiomyocytes were stimulated with 80 μg/ml of hAFS-CM and with 1 μg/well of hAFS-EV over vehicle control solution (Ctrl, serum-free medium - SF - used as negative control). R26pFUCCI2 mNVCM undergoing hAFS secretome stimulation were evaluated by immunostaining as the percentage of sarcomeric actinin alpha (αAct)-positive cardiomyocytes with nuclear signal of the mVenus probe marking the engagement of cell cycle activity (from phase S up to completion of phase M); primary mNVCM showed 50% enrichment of αAct-positive cardiomyocytes in respect to contaminating non-cardiomyocyte cells (i.e. cardiac fibroblasts, epicardial, and endothelial cells, as obtained from enzymatic digestion of the neonatal heart). R26pFUCCI2 mNVCM showed to be significantly responsive only to fetal hAFS-EVs, showing an increased progression to the M-phase by 2-fold (*$p<0.05$) as compared to untreated cells (Ctrl) (Figure 29). Fetal hAFS-CM treatment, in contrast to perinatal secretome, exhibited a positive trend in the increase of mNVCM M-phase progression when compared to Ctrl.

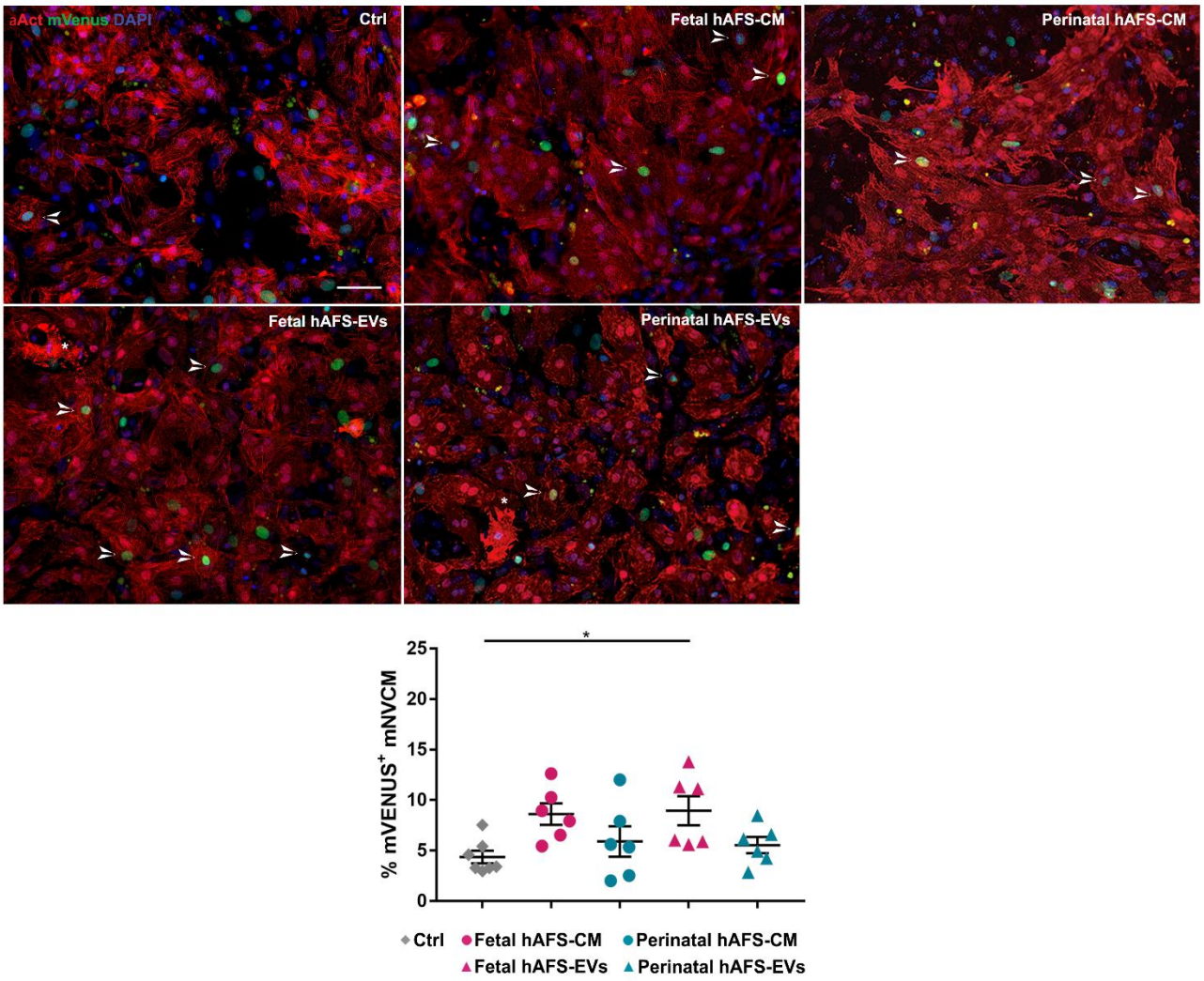

Figure 29 **Analysis of mNVCM cell cycle re-entry into M-phase following stimulation with hypoxic hAFS-CM and hAFS-EVs.** Upper panel: representative pictures of R26pFUCCI2 mNVCM in control conditions (Ctrl) or following treatment with fetal or perinatal hAFS-CM and fetal or perinatal hAFS-EVs stained with mVenus (green), mCherry (Red), αAct (red), and DAPI (Blue), scale bar 50µm; left panel: analysis of αAct-positive cells exposed to 80 µg/ml of fetal or perinatal hAFS-CM and to 1 µg of fetal or perinatal hAFS-EVs compared to Ctrl (SF medium) treated cells (negative control). Lower panel: representative images of nuclear colocalization of mVenus (green) and AuBK (white) on mNVCM, scale bar 50µm. All values are expressed as percentage per field ± s.e.m. of n=6 experiments (Ctrl: 4.358 ± 0.6257; fetal hAFS-CM: 8.619 ± 1.059; perinatal hAFS-CM: 5.904 ± 1.508; fetal hAFS-EVs: 8.949 ± 1.446; perinatal hAFS-EVs: 5.537 ± 0.8046; *p=0.0455; n.s: not significant).

Notably, when carefully analyzing true cell division in the stimulated mNVCM by evaluation of cytokinesis via specific expression of the cleavage furrow marker AuBK, only fetal hAFS-EVs significantly enhanced mNVCM proliferation. Indeed, a 4.5-fold increase in the percentage of αAct-positive cardiomyocytes expressing AuBK at midbodies was detected over untreated cells (*$p<0.05$, Figure 30). These results prompt the further *in vivo* validation of fetal hAFS-EVs as the most promising formulation to enhance myocardial renewal potential following myocardial infarction.

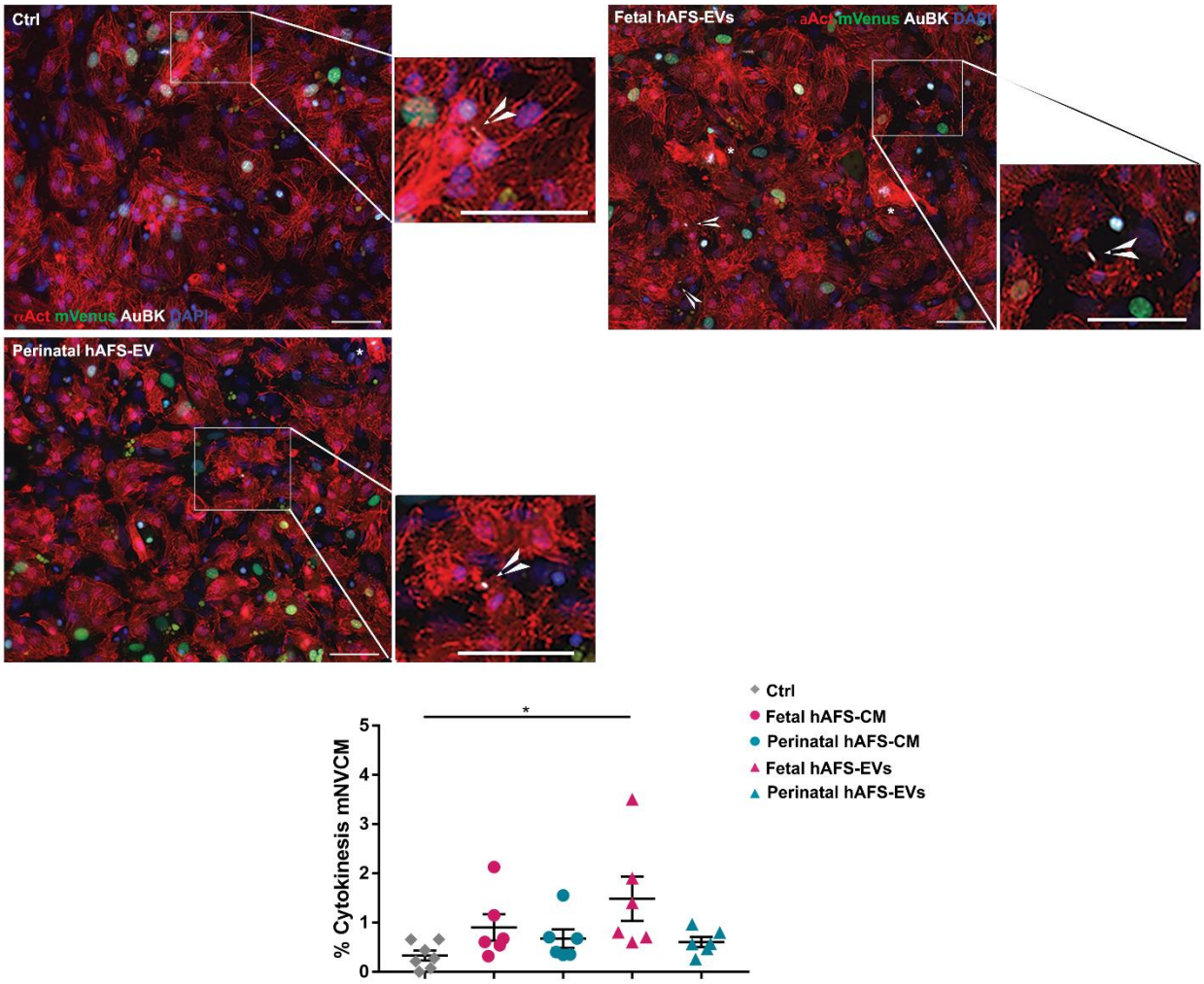

Figure 30 **Analysis of mNVCM cytokinesis following stimulation with hypoxic hAFS-CM and hAFS-EVs.** Upper panel**:** representative pictures of R26pFUCCI2 mNVCM in control conditions (Ctrl) or following treatment with fetal or perinatal hAFS-EVs stained with mCherry (Red) αAct (red), AuBK (white) and DAPI (Blue), scale bar 50µm; lower panel: analysis of αAct-positive cells exposed to 80µg/ml of fetal or perinatal hAFS-CM and to 1µg of fetal or perinatal hAFS-EVs compared to Ctrl (SF medium) treated cells (negative control). All values are expressed as percentage per field ± s.e.m. and n=6 experiments (Ctrl: 0.3312 ± 0.09988; fetal hAFS-CM: 0.9013 ± 0.2692; perinatal hAFS-CM: 0.6714 ± 0.1875; fetal hAFS-EVs: 1.483 ± 0.4512; perinatal hAFS-EVs: 0.6034 ± 0.102; *p=0.0202; n.s. not significant).

5 DISCUSSION

Leftover discarded samples of human amniotic fluid have been lately identified to be a valuable source of immature stromal cells with promising potential in the field of regenerative medicine and tissue engineering. Ethical concerns associated with their isolation are minimal, since they can be obtained from either leftover samples of routine prenatal screening amniocentesis, during the II trimester of gestation (fetal hAFS), or from amniotic fluid, discarded as clinical waste in III trimester scheduled C-section procedures (perinatal hAFS). hAFS have attracted significant interest as potential therapeutics for human tissue repair and regeneration, given the increasing evidence about their efficacy, obtained from experimental disease models.

The recent development of less invasive prenatal diagnostic techniques may result in a decrease in amniocentesis procedures in the near future, thus advocating perinatal hAFS as a more accessible option. Nevertheless, being fetal hAFS more developmentally immature they may harbor a more powerful paracrine potential. Against such scenario, in this study an accurate characterization of the fetal- and perinatal c-KIT$^+$ hAFS - including their secretome fractions - has been reported. From the results obtained in this study, it was possible to highlight some specific distinctions that can provide useful information for the possible clinical translation of their paracrine capacity.

Gestational stage did not influence hAFS phenotype; both fetal- and perinatal hAFS did not display a pro-senescent phenotype, and both cells expressed CD107a$^+$ and CD146$^+$ marker signature, which has been recently shown to define stromal progenitors with high secretory potency[57]. Both fetal and perinatal cells showed comparable morphology, while their metabolic activity revealed some differences. Fetal hAFS were characterized by an inefficient aerobic metabolism, while more mature perinatal ones showed higher oxygen consumption rate and ATP synthesis. This may suggest a more immature and "developmentally younger" metabolic profile of II trimester hAFS, resembling mesenchymal stromal cells isolated from the umbilical cord of preterm newborns, which have been shown to display the same trend [62].

When considering the cell behavior under the preconditioning previously validated to trigger their paracrine potential[4,5,63], fetal- and perinatal hAFS presented a positive trend in the increase of their secretome fraction concentration and in the amount of released EVs. Gestational stage did not exert any effect on the cell secretome yield nor on EV morphology and size distribution, as being equivalent between the two cell groups. Similarly, the appearance of fetal and perinatal hAFS and their corresponding secretome formulations was equivalent. Of note, the profiling of their paracrine cargo revealed some specific differences according to the distinct conditions that have been evaluated.

Indeed, fetal hAFS showed to be more responsive to the hypoxic preconditioning strategy, and exclusively enriched their conditioned medium with Angiogenin, EMMPRIM, IL-8 and MCP-1, as predictors of vascular regenerative efficacy[64]. This supports previous evidence of the paracrine potency of fetal hAFS-CM in boosting endogenous new vessel formation in preclinical rodent models of myocardial infarction, hind-limb ischemia, and ischemic fascio-cutaneous flap[5,65–67]. Besides, the fetal hAFS total secretome was found significantly enriched in IGFBP2 and OPN as compared to the perinatal one, thus suggesting a more pronounced pro-resolving and anti-aging modulatory profile[68–71]. While being less enhanced in paracrine factors, yet the perinatal hAFS-CM was similarly supplemented with neurotrophic and immunomodulatory factors, such as CST3 [72,73] and MIF [64]. Compared to hAFS-CM, the corresponding hypoxic fetal- and perinatal EV counterparts displayed a lower expression of cytokines and chemokines, except for the vascular remodeling mediator EMMPRIN [74], which was mostly enriched in the vesicle compartment. The previously reported cardio-active and pro-regenerative profile of fetal hAFS-EVs [3,5] has been here confirmed by the evidence of their exclusive expression of cardioprotective IL-8[75] and GDF-15, a key paracrine factor triggering endogenous adult hippocampal neurogenesis[76,77], as well as counteracting anthracycline-induced cardiotoxicity[64]. Both fetal- and perinatal hAFS-EVs showed similar expression of the progenitor/stem cell trafficking regulator SDF-1a [78–80]. This may explain previous results on the endothelial regenerative properties of III trimester hAFS in a preclinical mouse model of skeletal muscle ischemic injury[40], despite the obtained evidence of their hAFS-CM being less pro-angiogenic than the corresponding fetal one. Notably, the neural growth factor BDNF was found in both the fetal and perinatal EV cargo, although being expressed in low amounts, thus suggesting a putative neurotrophic activity for hAFS-EVs in influencing neuronal survival and neurodevelopmental processes, as recently reported for extracellular vesicles secreted by human bone marrow- and umbilical cord blood-derived MSC[81,82]. Notably, both secretome formulations from fetal and perinatal hAFS undergoing hypoxic stimulation showed to be enriched with PAI-1, a facilitator of endothelial activation[83] that is also involved in the M2 polarization of macrophages in the heart and endowed with cardioprotective and anti-fibrotic potential[84].

One of the most challenging targets in cardiac regenerative medicine is represented by obtaining myocardial renewal by means of effective cardiomyocyte proliferation. As a matter of fact, it has been reported that the early neonatal mouse heart retains endogenous regenerative response following injury, mainly through the dedifferentiation and proliferation of existing cardiomyocytes [37]. Therefore, it would be relevant to harness such regenerative potential by supporting it and extending it from the early neonatal stages up to the adult age. Considering that paracrine factors (including EVs) released from stem/progenitor cells have been shown to exert a cardio-active influence on

cardiovascular cells and cardiomyocytes, the secretome of developmentally juvenile cells, such as hAFS, may represent an interesting source to be investigated for such purpose, with the aim of rejuvenating and enhancing cardiomyocyte proliferative potential. Previous results obtained from prof. Bollini's team supported the evidence that the fetal hAFS secretome fractions (i.e. hAFS-CM and hAFS-EVs) can positively influence cardiomyocyte cell cycle re-entry in a preclinical adult mouse model of MI, with increased incorporation of bromodeoxyuridine (BrdU), thus suggesting a capability of myocardial renewal mechanisms[5]. However, cardiomyocyte BrdU incorporation per se may indicate cell cycle promotion limited to the DNA-duplication phase, without engagement into cell duplication and division.

In this study, this approach was further optimized *in vitro* by considering two main aspects:

(a) the use of a much more reliable system to trace murine cardiomyocyte cell cycle re-entry by the FUCCI technology, that is by genetically labelling with mutually exclusive fluorescent nuclear probes the progression from G1 into phase S and up to commitment into mitosis;

(b) the comparison of the cardio-active paracrine potential of the fetal and perinatal hAFS secretome formulations, in order to identify the most suitable hAFS source for possible therapeutic exploitation.

Interestingly, the results obtained *in vitro* showed a significant 2-fold increase in murine cardiomyocyte progression from S- up to M-phase only following paracrine stimulation with fetal hAFS-EVs, among all treatments tested (that is, by direct comparison with fetal hAFS-CM, perinatal hAFS-CM and perinatal hAFS-EVs). Moreover, the treatment with fetal hAFS-EVs enhanced by 4.5-fold the cytokinetic events of cardiomyocytes as a proof of bona fide cell division. The evidence that only the more immature fetal hAFS-EVs were able to significantly stimulate murine cardiomyocytes to divide may be related to their exclusive enrichment in agrin, as shown by proteomic analysis. Indeed, agrin is an extracellular matrix protein well known to concur to support cardiomyogenic events and myocardial renewal in the neonatal mouse heart after injury[6].

6 CONCLUSIONS

Overall, the results obtained in this work may provide useful insights in the paracrine potential of human amniotic fluid-derived stem cells (hAFS). In particular, for the first time a detailed comparison of more immature II trimester fetal hAFS (as obtained by prenatal screening amniocentesis procedures) versus late III trimester perinatal hAFS (as isolated from clinical waste material during scheduled C-section delivery) has been provided. Indeed, this study concurred to propose hAFS as an appealing source for future paracrine therapy in regenerative medicine, since they can be easily obtained during pregnancy or at term from leftover prenatal screening samples/clinical waste, they can be easily expanded without any significant alterations and primed *in vitro* to boost their paracrine potential.

Notably, while gestational stage may not impact on the cell phenotype and their secretory yield, specific differences in their metabolic activity and in the paracrine profile of their secretome formulations can be appreciated. As a matter of fact, developmentally younger fetal hAFS showed to produce secretome formulations with more pronounced pro-vasculogenic, pro-resolving and rejuvenating potential. Nevertheless, perinatal hAFS demonstrated to release paracrine factors important in endothelial cell migration, immune-modulation, anti-inflammatory and neurotrophic effects, similar to fetal hAFS. Therefore, these findings may be informative for future paracrine therapy of injury-related and inflammatory/ischemic-based disease. More in particular, when considering the cardiac regenerative scenario, fetal hAFS have shown to possess a more effective paracrine potential in sustaining cardiomyocyte proliferation, especially by means of their EV secretome fraction. Although these results seem promising, additional investigations are required to comprehensively analyse *in vivo* the myocardial renewal response driven by fetal hAFS-EV in a preclinical neonatal murine model of myocardial infarction, so to further validate these findings and provide a specific mechanism of action underlying this effect (such analyses are currently still ongoing and cannot be presented here, as being delayed by the Covid-19 pandemic which has affected the experimental plan of this study in the last year).

REFERENCES

1. Mirotsou M, Jayawardena TM, Schmeckpeper J, Gnecchi M, Dzau VJ. Paracrine mechanisms of stem cell reparative and regenerative actions in the heart. *J Mol Cell Cardiol*. 2011;50(2):280-289. doi:10.1016/j.yjmcc.2010.08.005

2. Gnecchi M, Zhang Z, Ni A, Dzau VJ. Paracrine mechanisms in adult stem cell signaling and therapy. *Circ Res*. 2008;103(11):1204-1219. doi:10.1161/CIRCRESAHA.108.176826

3. Balbi C, Piccoli M, Barile L, et al. First characterization of human amniotic fluid stem cell extracellular vesicles as a powerful paracrine tool endowed with regenerative potential. *Stem Cells Transl Med*. 2017;6(5):1340-1355. doi:10.1002/sctm.16-0297

4. Lazzarini E, Balbi C, Altieri P, et al. The human amniotic fluid stem cell secretome effectively counteracts doxorubicin-induced cardiotoxicity. *Sci Rep*. 2016;6. doi:10.1038/srep29994

5. Balbi C, Lodder K, Costa A, et al. Reactivating endogenous mechanisms of cardiac regeneration via paracrine boosting using the human amniotic fluid stem cell secretome. *Int J Cardiol*. 2019;287:87-95. doi:10.1016/j.ijcard.2019.04.011

6. Bassat E, Mutlak YE, Genzelinakh A, et al. The extracellular matrix protein agrin promotes heart regeneration in mice. *Nature*. 2017;547(7662):179-184. doi:10.1038/nature22978

7. Mao AS, Mooney DJ. Regenerative medicine: Current therapies and future directions. *Proc Natl Acad Sci U S A*. 2015;112(47):14452-14459. doi:10.1073/pnas.1508520112

8. Bollini S, Smits AM, Balbi C, Lazzarini E, Ameri P. Triggering endogenous cardiac repair and regeneration via extracellular vesicle-mediated communication. *Front Physiol*. 2018;9(OCT). doi:10.3389/fphys.2018.01497

9. Baraniak PR, McDevitt TC. Stem cell paracrine actions and tissue regeneration. *Regen Med*. 2010;5(1):121-143. doi:10.2217/rme.09.74

10. Bollini S, Cheung KK, Riegler J, et al. Amniotic fluid stem cells are cardioprotective following acute myocardial infarction. *Stem Cells Dev*. 2011;20(11):1985-1994. doi:10.1089/scd.2010.0424

11. Wagers AJ, Weissman IL. Plasticity of adult stem cells. *Cell*. 2004;116(5):639-648. doi:10.1016/S0092-8674(04)00208-9

12. Bollini S, Gentili C, Tasso R, Cancedda R. The Regenerative Role of the Fetal and Adult Stem Cell Secretome. *J Clin Med*. 2013;2(4):302-327. doi:10.3390/jcm2040302

13. Cantaluppi V, Biancone L, Quercia A, Deregibus MC, Segoloni G, Camussi G. Rationale of mesenchymal stem cell therapy in kidney injury. *Am J Kidney Dis*. 2013;61(2):300-309. doi:10.1053/j.ajkd.2012.05.027

14. Kuo TK, Hung SP, Chuang CH, et al. Stem Cell Therapy for Liver Disease: Parameters Governing the Success of Using Bone Marrow Mesenchymal Stem Cells. *Gastroenterology*. 2008;134(7). doi:10.1053/j.gastro.2008.03.015

15. Lee JW, Fang X, Krasnodembskaya A, Howard JP, Matthay MA. Concise review: Mesenchymal stem cells for acute lung injury: Role of paracrine soluble factors. *Stem Cells*. 2011;29(6):913-919. doi:10.1002/stem.643

16. Uccelli A, Benvenuto F, Laroni A, Giunti D. Neuroprotective features of mesenchymal stem cells. *Best Pract Res Clin Haematol*. 2011;24(1):59-64. doi:10.1016/j.beha.2011.01.004

17. Roger VL. Epidemiology of heart failure. *Circ Res*. 2013;113(6):646-659. doi:10.1161/CIRCRESAHA.113.300268

18. Madonna R, Van Laake LW, Davidson SM, et al. Position Paper of the European Society of Cardiology Working Group Cellular Biology of the Heart: Cell-based therapies for myocardial repair and regeneration in ischemic heart disease and heart failure. *Eur Heart J*. 2016;37(23):1789-1798. doi:10.1093/eurheartj/ehw113

19. Paoletti C, Divieto C, Chiono V. Impact of Biomaterials on Differentiation and Reprogramming Approaches for the Generation of Functional Cardiomyocytes. *Cells*. 2018;7(9):114. doi:10.3390/cells7090114

20. Sid-Otmane C, Perrault LP, Ly HQ. Mesenchymal stem cell mediates cardiac repair through autocrine, paracrine and endocrine axes. *J Transl Med*. 2020;18(1). doi:10.1186/s12967-020-02504-8

21. Vadivel S, Vincent P, Sekaran S, et al. Inflammation in myocardial injury- Stem cells as potential immunomodulators for myocardial regeneration and restoration. *Life Sci*. 2020;250. doi:10.1016/j.lfs.2020.117582

22. Gnecchi M, Danieli P, Cervio E. Mesenchymal stem cell therapy for heart disease. *Vascul Pharmacol*. 2012;57(1):48-55. doi:10.1016/j.vph.2012.04.002

23. Gnecchi M, Danieli P, Malpasso G, Ciuffreda MC. Paracrine mechanisms of mesenchymal stem cells in tissue repair. In: *Methods in Molecular Biology*. Vol 1416. Humana Press Inc.; 2016:123-146. doi:10.1007/978-1-4939-3584-0_7

24. Gnecchi M, He H, Noiseux N, et al. Evidence supporting paracrine hypothesis for Akt-modified mesenchymal stem cell-mediated cardiac protection and functional improvement. *FASEB J*. 2006;20(6):661-669. doi:10.1096/fj.05-5211com

25. Théry C, Witwer KW, Aikawa E, et al. Minimal information for studies of extracellular vesicles 2018 (MISEV2018): a position statement of the International Society for Extracellular Vesicles and update of the MISEV2014 guidelines. *J Extracell Vesicles*. 2018;7(1). doi:10.1080/20013078.2018.1535750

26. Bruno S, Kholia S, Deregibus MC, Camussi G. The role of extracellular vesicles as paracrine effectors in stem cell-based therapies. In: *Advances in Experimental Medicine and Biology*. Vol 1201. Springer; 2019:175-193. doi:10.1007/978-3-030-31206-0_9

27. Kalra H, Drummen GPC, Mathivanan S. Focus on extracellular vesicles: Introducing the next small big thing. *Int J Mol Sci*. 2016;17(2):170. doi:10.3390/ijms17020170

28. Balbi C, Costa A, Barile L, Bollini S. Message in a Bottle: Upgrading Cardiac Repair into Rejuvenation. *Cells*. 2020;9(3):724. doi:10.3390/cells9030724

29. Lai RC, Arslan F, Lee MM, et al. Exosome secreted by MSC reduces myocardial ischemia/reperfusion injury. *Stem Cell Res*. 2010;4(3):214-222. doi:10.1016/j.scr.2009.12.003

30. Ratajczak J, Kucia M, Mierzejewska K, et al. Paracrine proangiopoietic effects of human umbilical cord blood-derived purified CD133+ cells-implications for stem cell therapies in regenerative medicine. *Stem Cells Dev*. 2013;22(3):422-430. doi:10.1089/scd.2012.0268

31. Barile L, Vassalli G. Exosomes: Therapy delivery tools and biomarkers of diseases. *Pharmacol Ther*. 2017;174:63-78. doi:10.1016/j.pharmthera.2017.02.020

32. Kalluri R, LeBleu VS. The biology, function, and biomedical applications of exosomes. *Science (80-)*. 2020;367(6478). doi:10.1126/science.aau6977

33. Günthel M, Barnett P, Christoffels VM. Development, Proliferation, and Growth of the Mammalian Heart. *Mol Ther*. 2018;26(7):1599-1609. doi:10.1016/j.ymthe.2018.05.022

34. Eschenhagen T, Bolli R, Braun T, et al. Cardiomyocyte regeneration: A consensus statement. *Circulation*. 2017;136(7):680-686. doi:10.1161/CIRCULATIONAHA.117.029343

35. Bergmann O, Bhardwaj RD, Bernard S, et al. Evidence for cardiomyocyte renewal in humans. *Science (80-)*. 2009;324(5923):98-102. doi:10.1126/science.1164680

36. Porrello ER, Mahmoud AI, Simpson E, et al. Transient regenerative potential of the neonatal mouse heart. *Science (80-)*. 2011;331(6020):1078-1080. doi:10.1126/science.1200708

37. Xin M, Olson EN, Bassel-Duby R. Mending broken hearts: Cardiac development as a basis for adult heart regeneration and repair. *Nat Rev Mol Cell Biol*. 2013;14(8):529-541. doi:10.1038/nrm3619

38. Bollini S, Silini AR, Banerjee A, Wolbank S, Balbi C, Parolini O. Cardiac restoration stemming from the placenta tree: Insights from fetal and perinatal cell biology. *Front Physiol*. 2018;9(APR). doi:10.3389/fphys.2018.00385

39. Balbi C, Bollini S. Fetal and perinatal stem cells in cardiac regeneration: Moving forward to the paracrine era. *Placenta*. 2017;59:96-106. doi:10.1016/j.placenta.2017.04.008

40. Schiavo AA, Franzin C, Albiero M, et al. Endothelial properties of third-Trimester amniotic fluid stem cells

cultured in hypoxia. *Stem Cell Res Ther*. 2015;6(1). doi:10.1186/s13287-015-0204-0

41. De Coppi P, Bartsch G, Siddiqui MM, et al. Isolation of amniotic stem cell lines with potential for therapy. *Nat Biotechnol*. 2007;25(1):100-106. doi:10.1038/nbt1274

42. Santos DS dos, Goldenberg RC dos S. Doxorubicin-Induced Cardiotoxicity: From Mechanisms to Development of Efficient Therapy. In: *Cardiotoxicity*. InTech; 2018. doi:10.5772/intechopen.79588

43. Mellows B, Mitchell R, Antonioli M, et al. Protein and Molecular Characterization of a Clinically Compliant Amniotic Fluid Stem Cell-Derived Extracellular Vesicle Fraction Capable of Accelerating Muscle Regeneration Through Enhancement of Angiogenesis. *Stem Cells Dev*. 2017;26(18):1316-1333. doi:10.1089/scd.2017.0089

44. Antounians L, Tzanetakis A, Pellerito O, et al. The Regenerative Potential of Amniotic Fluid Stem Cell Extracellular Vesicles: Lessons Learned by Comparing Different Isolation Techniques. *Sci Rep*. 2019;9(1):1-11. doi:10.1038/s41598-018-38320-w

45. Zavatti M, Beretti F, Casciaro F, Bertucci E, Maraldi T. Comparison of the therapeutic effect of amniotic fluid stem cells and their exosomes on monoiodoacetate-induced animal model of osteoarthritis. *BioFactors*. 2020;46(1):106-117. doi:10.1002/biof.1576

46. Gatti M, Beretti F, Zavatti M, et al. Amniotic Fluid Stem Cell-Derived Extracellular Vesicles Counteract Steroid-Induced Osteoporosis In Vitro. *Int J Mol Sci*. 2020;22(1):38. doi:10.3390/ijms22010038

47. Li B, Lee C, O'Connell JS, et al. Activation of Wnt signaling by amniotic fluid stem cell-derived extracellular vesicles attenuates intestinal injury in experimental necrotizing enterocolitis. *Cell Death Dis*. 2020;11(9):1-12. doi:10.1038/s41419-020-02964-2

48. Sedrakyan S, Villani V, Da Sacco S, et al. Amniotic fluid stem cell-derived vesicles protect from VEGF-induced endothelial damage. *Sci Rep*. 2017;7(1):1-12. doi:10.1038/s41598-017-17061-2

49. Pös O, Budiš J, Szemes T. Recent trends in prenatal genetic screening and testing [version 1; peer review: 2 approved]. *F1000Research*. 2019;8. doi:10.12688/f1000research.16837.1

50. Di Trapani M, Bassi G, Fontana E, et al. Immune regulatory properties of CD117pos amniotic fluid stem cells vary according to gestational age. *Stem Cells Dev*. 2015;24(1):132-143. doi:10.1089/scd.2014.0234

51. Ma J, Zhao Y, Sun L, et al. Exosomes Derived from Akt -Modified Human Umbilical Cord Mesenchymal Stem Cells Improve Cardiac Regeneration and Promote Angiogenesis via Activating Platelet-Derived Growth Factor D . *Stem Cells Transl Med*. 2017;6(1):51-59. doi:10.5966/sctm.2016-0038

52. Ni J, Liu X, Yin Y, Zhang P, Xu YW, Liu Z. Exosomes derived from TIMP2-modified human umbilical cord mesenchymal stem cells enhance the repair effect in rat model with myocardial infarction possibly by the Akt/ SFRP2 pathway. *Oxid Med Cell Longev*. 2019;2019. doi:10.1155/2019/1958941

53. Gong XH, Liu H, Wang SJ, Liang SW, Wang GG. Exosomes derived from SDF1-overexpressing mesenchymal stem cells inhibit ischemic myocardial cell apoptosis and promote cardiac endothelial microvascular regeneration in mice with myocardial infarction. *J Cell Physiol*. 2019;234(8):13878-13893. doi:10.1002/jcp.28070

54. Komaki M, Numata Y, Morioka C, et al. Exosomes of human placenta-derived mesenchymal stem cells stimulate angiogenesis. *Stem Cell Res Ther*. 2017;8(1):219. doi:10.1186/s13287-017-0660-9

55. Du W, Zhang K, Zhang S, et al. Enhanced proangiogenic potential of mesenchymal stem cell-derived exosomes stimulated by a nitric oxide releasing polymer. *Biomaterials*. 2017;133:70-81. doi:10.1016/j.biomaterials.2017.04.030

56. Itahana K, Campisi J, Dimri GP. Methods to Detect Biomarkers of Cellular Senescence. In: *Methods in Molecular Biology (Clifton, N.J.)*. Vol 371. Methods Mol Biol; 2007:21-31. doi:10.1007/978-1-59745-361-5_3

57. Bowles AC, Kouroupis D, Willman MA, Perucca Orfei C, Agarwal A, Correa D. Signature quality attributes of CD146+ mesenchymal stem/stromal cells correlate with high therapeutic and secretory potency. *Stem Cells*. 2020;38(8):1034-1049. doi:10.1002/stem.3196

58. Hinkle PC. P/O ratios of mitochondrial oxidative phosphorylation. *Biochim Biophys Acta - Bioenerg*. 2005;1706(1-2):1-11. doi:10.1016/j.bbabio.2004.09.004

59. Abe T, Sakaue-Sawano A, Kiyonari H, et al. Visualization of cell cycle in mouse embryos with Fucci2 reporter directed by Rosa26 promoter. *Dev*. 2013;140(1):237-246. doi:10.1242/dev.084111

60. Preston S, Aras S, Zaidi M. Spatiotemporal Labeling of Melanocytes in Mice. *Int J Mol Sci*. 2018;19(5):1469. doi:10.3390/ijms19051469

61. Balbi C, Lodder K, Costa A, et al. Supporting data on in vitro cardioprotective and proliferative paracrine effects by the human amniotic fluid stem cell secretome. *Data Br*. 2019;25:104324. doi:10.1016/j.dib.2019.104324

62. Ravera S, Podestà M, Sabatini F, et al. Mesenchymal stem cells from preterm to term newborns undergo a significant switch from anaerobic glycolysis to the oxidative phosphorylation. *Cell Mol Life Sci*. 2018;75(5):889-903. doi:10.1007/s00018-017-2665-z

63. Kukumberg M, Phermthai T, Wichitwiengrat S, et al. Hypoxia-induced amniotic fluid stem cell secretome augments cardiomyocyte proliferation and enhances cardioprotective effects under hypoxic-ischemic conditions. *Sci Rep*. 2021;11(1):163. doi:10.1038/s41598-020-80326-w

64. Zhang Y, Liang X, Liao S, et al. Potent Paracrine Effects of human induced Pluripotent Stem Cell-derived Mesenchymal Stem Cells Attenuate Doxorubicin-induced Cardiomyopathy. *Sci Rep*. 2015;5. doi:10.1038/srep11235

65. Mirabella T, Poggi A, Scaranari M, et al. Recruitment of host’s progenitor cells to sites of human amniotic fluid stem cells implantation. *Biomaterials*. 2011;32:4218-4227. doi:10.1016/j.biomaterials.2010.12.028

66. Mirabella T, Cilli M, Carlone S, et al. Amniotic liquid derived stem cells as reservoir of secreted angiogenic factors capable of stimulating neo-arteriogenesis in an ischemic model. *Biomaterials*. 2011;32(15):3689-3699. doi:10.1016/j.biomaterials.2011.01.071

67. Mirabella T, Hartinger J, Lorandi C, Gentili C, Van Griensven M, Cancedda R. Proangiogenic Soluble Factors from Amniotic Fluid Stem Cells Mediate the Recruitment of Endothelial Progenitors in a Model of Ischemic Fasciocutaneous Flap. doi:10.1089/scd.2011.0639

68. Azar WJ, Azar SHX, Higgins S, et al. IGFBP-2 enhances VEGF gene promoter activity and consequent promotion of angiogenesis by neuroblastoma cells. *Endocrinology*. 2011;152(9):3332-3342. doi:10.1210/en.2011-1121

69. Aslam M, Baveja R, Liang OD, et al. Bone marrow stromal cells attenuate lung injury in a murine model of neonatal chronic lung disease. *Am J Respir Crit Care Med*. 2009;180(11):1122-1130. doi:10.1164/rccm.200902-0242OC

70. Wang W, Li P, Li W, et al. Osteopontin activates mesenchymal stem cells to repair skin wound. *PLoS One*. 2017;12(9). doi:10.1371/journal.pone.0185346

71. Guidi N, Sacma M, Ständker L, et al. Osteopontin attenuates aging-associated phenotypes of hematopoietic stem cells. *EMBO J*. 2017;36(7):840-853. doi:10.15252/embj.201694969

72. Wang XF, Liu DX, Liang Y, et al. Cystatin C Shifts APP processing from amyloid-β production towards non-Amyloidgenic pathway in brain endothelial Cells. *PLoS One*. 2016;11(8). doi:10.1371/journal.pone.0161093

73. Taupin P, Ray J, Fischer WH, et al. FGF-2-responsive neural stem cell proliferation requires CCg, a novel autocrine/paracrine cofactor. *Neuron*. 2000;28(2):385-397. doi:10.1016/S0896-6273(00)00119-7

74. Vrijsen KR, Maring JA, Chamuleau SAJ, et al. Exosomes from Cardiomyocyte Progenitor Cells and Mesenchymal Stem Cells Stimulate Angiogenesis Via EMMPRIN. *Adv Healthc Mater*. 2016;5(19):2555-2565. doi:10.1002/adhm.201600308

75. Peng KY, Liu YH, Li YW, Yen BL, Yen ML. Extracellular matrix protein laminin enhances mesenchymal stem cell (MSC) paracrine function through αvβ3/CD61 integrin to reduce cardiomyocyte apoptosis. *J Cell Mol Med*. 2017;21(8):1572-1583. doi:10.1111/jcmm.13087

76. Kim DH, Lee D, Chang EH, et al. GDF-15 secreted from human umbilical cord blood mesenchymal stem cells delivered through the cerebrospinal fluid promotes hippocampal neurogenesis and synaptic activity in an Alzheimer's disease model. *Stem Cells Dev*. 2015;24(20):2378-2390. doi:10.1089/scd.2014.0487

77. Kim DH, Lee D, Lim H, et al. Effect of growth differentiation factor-15 secreted by human umbilical cord blood-derived mesenchymal stem cells on amyloid beta levels in in vitro and in vivo models of Alzheimer's disease. *Biochem Biophys Res Commun*. 2018;504(4):933-940. doi:10.1016/j.bbrc.2018.09.012

78. Marquez-Curtis LA, Janowska-Wieczorek A. Enhancing the migration ability of mesenchymal stromal cells by targeting the SDF-1/CXCR4 axis. *Biomed Res Int*. 2013;2013. doi:10.1155/2013/561098

79. Chen L, Li Y, Chen W, et al. Enhanced recruitment and hematopoietic reconstitution of bone marrow-derived mesenchymal stem cells in bone marrow failure by the SDF-1/CXCR4. *J Tissue Eng Regen Med*. 2020;14(9):1250-1260. doi:10.1002/term.3096

80. Wang G, Zhuo Z, Zhang Q, et al. Transfection of CXCR-4 Using Microbubble-Mediated Ultrasound Irradiation and Liposomes Improves the Migratory Ability of Bone Marrow Stromal Cells. *Curr Gene Ther*. 2014;15(1):21-31. doi:10.2174/1566523214666141121111220

81. Ahn SY, Sung DK, Kim YE, Sung S, Chang YS, Park WS. Brain-derived neurotropic factor mediates neuroprotection of mesenchymal stem cell-derived extracellular vesicles against severe intraventricular hemorrhage in newborn rats. *Stem Cells Transl Med*. Published online 2020. doi:10.1002/sctm.20-0301

82. Kaminski N, Köster C, Mouloud Y, et al. Mesenchymal Stromal Cell-Derived Extracellular Vesicles Reduce Neuroinflammation, Promote Neural Cell Proliferation and Improve Oligodendrocyte Maturation in Neonatal Hypoxic-Ischemic Brain Injury. *Front Cell Neurosci*. 2020;14. doi:10.3389/fncel.2020.601176

83. Isogai C, Laug WE, Shimada H, et al. Plasminogen activator inhibitor-1 promotes angiogenesis by stimulating endothelial cell migration toward fibronectin. *Cancer Res*. 2001;61(14):5587-5594.

84. Baumeier C, Escher F, Aleshcheva G, Pietsch H, Schultheiss HP. Plasminogen activator inhibitor-1 reduces cardiac fibrosis and promotes M2 macrophage polarization in inflammatory cardiomyopathy. *Basic Res Cardiol*. 2021;116(1):1. doi:10.1007/s00395-020-00840-w

ACKNOWLEDGEMENTS

I would like to express my deep and sincere gratitude to my research supervisor Prof. Sveva Bollini, Regenerative Medicine Laboratory, Biology Unit, Department of Experimental Medicine, for giving me the opportunity to participate and contribute to this interesting project guiding and teaching me the methodology to carry out the research and present the research works as clearly as possible. I thank my co-supervisor who assisted me Professor Silvia Ravera, from the Human Anatomy Unit, Department of Experimental Medicine, who assisted me in part of this work.

A special thanks is addressed to Dr. Ambra Costa, PhD student, for guiding me with enthusiasm and passion in the practical part of this work and for helping me to face and to overcome research issues. I also thank Dr. Patrizia Garbati, Post Doc research fellow, and the all Regenerative Medicine Laboratory staff, who also assisted me in case of need.

I also thank all the people who contributed to this study: Antonella De Palma and Pierluigi Mauri, C.N.R. - .I.T.B. Institute for Biomedical Technologies National Research Council Proteomics and Metabolomics Unit for proteomic analysis; Katia Cortese and Sara Santamaria, Human Anatomy Unit, Department of Experimental Medicine, for extracellular vesicles characterization by TEM; Carolina Balbi, Laboratory of Cellular and Molecular Cardiology, Cardiocentro Ticino Foundation, for extracellular vesicles characterization by by NTA analysis; Daniele Reverberi Molecular Pathology Unit, IRCCS Ospedale Policlinico, San Martino, for cytofluorimetric analysis; Pierangela De Biasio, Prenatal Diagnosis and Perinatal Medicine Unit, IRCCS Ospedale Policlinico San Martino, Dario Paladini, Fetal Medicine and Surgery Unit, IRCCS Istituto Giannina Gaslini, Domenico Coviello, Human Genetics Unit, IRCCS Istituto Giannina Gaslini for the supply of left-over human amniotic fluid samples.

I would like to say thanks to my friends and classmates Chiara Giordano and Edra Jaho, without whom this achievement would have been much more difficult, thanks for having supported and put up with me, and for the worst moments that you have been able to turn into occasion of laughter.

Finally, my thanks go to my family and my boyfriend, who are the people closest to me. Thanks for believing in me as I can't, to you I owe everything. Thanks to my granny Mariuccia, who will be in my heart forever.